International Journal of Antennas and Propagation

Antennas and Propagation for 6G Wireless Communications

Lead Guest Editor: Sami Myllymäki
Guest Editors: George C. Alexandropoulos and A. Sali

Antennas and Propagation for 6G Wireless Communications

International Journal of Antennas and Propagation

Antennas and Propagation for 6G Wireless Communications

Lead Guest Editor: Sami Myllymäki
Guest Editors: George C. Alexandropoulos and A. Sali

Contents

Hindawi
International Journal of Antennas and Propagation
Volume 2022, Article ID 8378526, 9 pages
https://doi.org/10.1155/2022/8378526

Research Article

A Novel Design of Hybrid Precoder in Multicell, Multiuser Heterogeneous Network

Mohammad Reza Pouryeganeh, Azim Fard, and Mohammad Bagher Tavakoli

Department of Electrical Engineering, Arak Branch, Islamic Azad University, Arak, Iran

Correspondence should be addressed to Azim Fard; azimfard@cra.ir

Received 28 November 2021; Revised 6 May 2022; Accepted 1 July 2022; Published 18 August 2022

Academic Editor: Giuseppe Castaldi

In this paper, the precoders capable of maximizing the weighted sum rate (WSR) for multicell scenarios under power budget constraint conditions per cell were considered based on the MIMO system performance. This rate is strongly affected by intracellular interference, so we recommend using coordinated beam forming (CBF). If the number of user equipment provided per cell is small enough to the number of transmit antennas, simple linear beamformers, such as matched filter (MF), achieve higher performance rates. In general cases, two algorithms meet the best performance in terms of the total achievable rate; these are KG (Kim Giannakis) and WSMSE (Weighted Sum Minimum Squared Error) algorithms. In the KG method, the objective function of the sum rate is suggested to be divided into two functions, one function for the desired user rate and the other for the sum rate of the remaining users. In the WSMSE algorithm, maximizing the sum rate is solved by redefining it as the problem of minimizing the MSE (Mean Square Error) function. These functions are convex and nonconvex functions, respectively. In the proposed method, the WSMSEs were modified to reduce the complexity and calculations to provide optimal performance in beamforming.

1. Introduction

Using the MIMO systems has some advantages as they use dozens of terminals that can provide services to many users simultaneously and therefore increase the spectral efficiency (SE) [1–7]. On the other hand, as the number of users in cellular networks increases, intercell interference (ICI) increases in the system that causing detrimental effects on SE, so precoders are designed to eliminate intercell SE. Using the MIMO systems reduces on-air latency, which is one of the new generations of wireless communications in heterogeneous environments. Another effective instrument in 5G communication is the use of mmWaves. The bandwidth of mmWaves a range from 30 to 300 GHz is considered an alternative band to compensate for the lack of bandwidth in the physical layer in generating this cellular communication. To ensure mmWave systems coverage, an ultradense network is introduced as a promising technology to achieve high system capacity [8]. Using this frequency band based on the nature of the mmWave band, causes the number of wave reflections in contact with objects to be significantly reduced and increases the number of base stations, thereby increasing the potential for intercell and intracell interference.

Moreover, massive MIMO array antennas are applied as one of the central promises of high directional beamforming to deal with path loss due to the mmWave signals seriously. Using massive MIMO because of small fading, intercell, and intracell interference can be significantly reduced by addressing the phenomenon of pilot signal contamination [9–16]. Using linear precoders in multicell and singlecell scenarios has demonstrated that the total achievable rate can increase significantly concerning the ratio of BS antennas to the user. In recent years, many studies have been done on designing and using hybrid precoders too.

Unfortunately, for the mmWave, MIMO systems run with many antennas, digital processing is not cost-effective because it incurs substantial costs for the system hardware, resulting in many complications. Hybrid precoder architecture is provided where the signal is processed by both analog and digital precoders to reduce cost and provide

suitable performance [17–20]. Using a multiuser scenario, a hybrid precoder was examined by a greedy-like approach where a simultaneous orthogonal matching pursuit (SOMP) algorithm is proposed [19]. The methods mentioned above are based on the assumption of perfect channel state information and the availability of array response sets, i.e., F and W for precoder and combiner, respectively. These sets combine sending and receiving control vectors in the face of arrival/departure (DoA/DoD) where the users are stationed. In Alkhateeb et al., when a single RF chain is used in mobile phone users, the low-resolution analog-to-digital converters (ADCs) performance is examined, and in [21, 37], the nonconvex problem is solved by the inner-convex method. The findings have demonstrated that compared to traditional optimization techniques, l_0-norm relaxation techniques can significantly reduce interference compared to other techniques for eliminating cloud-radio access networks (C-RAN) interference. The authors [37] have presented a connected structure for a hybrid beamforming structure. An optimization problem is broken down into several subproblems consisting of precoder matrices with hybrid digital and analog precoders being created with an aggregate performance around near-optimal points through submatrices to precode each subarray. Hence, it seems to be a relatively tricky path in terms of complexity. In Chan et al. [22], it is shown that the Gram matrix of the frequency-selective channel can be broken down into frequency-flat and frequency-selective components as these components can be used in analog and base-band precoders. In Lin et al. [23], the channel matrix is broken down into an angular amplitude base matrix and a yield matrix, which fully correspond to the hybrid precoder structure. A hybrid precoding processor based on parallel-index-selection corresponding to matrix-inversion-free orthogonality has been proposed in the study by Lee et al. [24]. In Raghavan et al. [25], after directional precoded structures establish communications as a low-and high-complexity solution to meet data volume demand, a simple class of directional schedules based on channel structure is provided. Then, the performance between single- and multiuser scenarios is compared. In Ni and Dong [26, 38], for massive multiuser MIMO systems, a hybrid block diagonalization scheme has been suggested to approach the capacity performance of the baseband digital method. Generally, one would suggest many techniques that have been used to simplify the problem and create various hybrid precoder designs to create a suitable instrument to increase the SE. Castanheira et al [27] have tried to eliminate both inter/intratier interferences for uplink ultradense mmWave heterogeneous networks through the employment of low-feedback hybrid precoder-equalizer in the multicell massive MIMO systems. The analog part of the system has been optimized by minimizing the distance between the hybrid and the fully digital approaches [28]. Based on the dominance of interuser interference, intrauser interference, or both in downlink mmWave MIMO, nonlinear successive interference cancellation (SIC)-aided hybrid beamforming algorithms have been proposed with 2-bit finite resolution phase shifters that can achieve over 91% SE of infinite resolution phase shifters. Lavdas et al [29] presented an adaptive hybrid beamforming approach of the 5 G·mmWave cellular networks. The proposed scheme is the deployment of a separate RF chain connected per vertical antenna array, and a different set of antenna elements are active to perform radiation pattern formulation. Reducing total downlink transmission power due to hardware complexity reduction improves mmWave massive MIMO performance.

In this paper, we propose a multicell interference processing scheme for a hybrid precoder structure-based MIMO Broadcasting Channel. Inspired by the idea of signal subspace alignment and turning the basic equation into a convex equation to design a hybrid precoder, we reduce the signal-to-noise ratio (SNR) of each BS to reduce ICI with RF receivers and to develop a beamforming problem.

In Section 2, system model of our work is described in detail. We have the multicells, multiusers MIMO system whose rate is affected by intracellular interferences. Then, we define an optimization problem for precoding. In Section 3, we expose an WSMSE algorithm to solve the optimization problem because it is nonconcave in the precoding matrix. Using this method, two new matrices will be obtained to calculate the new precoder matrix. Another method to solve the optimization problem, KG precoder algorithm is exposed in Section 4. Because precoding optimization problem is highly nonconvergent. In the V-A section, DAV is used in the WSMSE and KG algorithms. Moreover, in the V-B section, we present a novel version of the WSMSE where the number of antennas is very large compared to the number of users named WSMSE, a New Form. All results are summarized in VI conclusions.

1.1. Notation. The following notation is adopted throughout the thesis: boldface upper symbols represent matrices and boldface lower symbols represent vectors. Scalars are denoted in lower case symbols. The transpose and conjugate transpose operators are denoted by $(.)^T$ and $(.)^H$, respectively. det(·), tr(·), and $(.)^{-1}$ denote the matrix determinant, trace, and inverse, respectively. E(·) denotes the expectation of a random variable. log(·) denotes the binary logarithm.

2. System Model

To eliminate interference and maximize SE, we consider the downlink multicell, multiuser MIMO scenario; in this scenario, there are C cells ($c = 1 \sim C$), each of which includes a BS with M antenna (we consider isotropic); these antennas transmit data to K users who are equipped with N antennas in Rxs. The received signal $\boldsymbol{y}_{c,k} \in C^{N\times 1}$ in user k in cell c is expressed as follows:

$$\mathbf{y}_{c,k} = \sum_{m=1}^{C}\sum_{l=1}^{K}\mathbf{H}_{m.c,k}\mathbf{G}_{m,l}\mathbf{s}_{m,l} + \mathbf{n}_{c,k}. \quad (1)$$

In the above relation, user symbols are selected as Gaussian codebooks (i.e., $\mathbf{s}_{m,l} \in \mathbb{C}^{d_{m,l},1}$), each element of which $\sim N\mathbb{C}(0,1)$ is linearly precoded, generating the transmitted signal. $d_{m,\ l}$ is the number of sequences permitted by user l of cell m. $\mathbf{G}_{m,l,} \in \mathbb{C}^{M\times d_{m,l}}$ is the precoding

vector of user l in cell m. $\mathbf{H}_{m.c,k} \in \mathbb{C}^{N\times M}$ is the channel matrix from the sender m to the user k of cell c. $\mathbf{n}_{c,k}$ of the next vector $\mathbb{C}^{N\times 1}$ involves independent mixed Gaussian noise expressions with mean zero and variance σ^2. Moreover, the covariance matrix of $\mathbf{H}_{i.c,k}$ channel is equal to $E[\mathbf{H}_{i,c,k}^H \mathbf{H}_{i,c,k}] = \Theta_{i,c,k}$. Because of the power budget constraint per Tx, the average power constraint is defined for the precoders. Thus,

$$tr\mathbf{G}_c\mathbf{G}_c^H \preccurlyeq P_c \; for \; c \in C, \tag{2}$$

where C is the set of all BSs. $\mathbf{G}_c = [\mathbf{G}_{c,1}, \mathbf{G}_{c,2}, \ldots, \mathbf{G}_{c,K}] \in \mathbb{C}^{M\times K}$ is the precoding matrix and P_c is the total transmitted power in cell c.

Assuming optimal singleuser coding and CSIT (Channel State Information at the Transmitter) and full CSI in the receivers of CSIR (Channel State Information at the Receiver), the achievable rate $r_{c,k}$ of user k of cell c is shown as follows:

$$\begin{aligned} r_{c,k} &= \log\det\left(\mathbf{I}_N + \Gamma_{c,k}\right), \\ \Gamma_{c,k} &= \mathbf{R}_{\widehat{c,k}}^{-1}\mathbf{H}_{c,c,k}\mathbf{Q}_{c,k}\mathbf{H}_{c,c,k}^H, \end{aligned} \tag{3}$$

where $\mathbf{Q}_{c,k} = \mathbf{G}_{c,k}\mathbf{G}_{c,k}^H$ is the transmission covariance matrix; $\boldsymbol{\Gamma}_{c,k}$ is the ratio of signal to interference along with the (SINR) noise of user k of cell c; and $\mathbf{R}_{\widehat{c,k}}^{-1}$ is the covariance matrix of the interference along with the noise received by user k of cell c, which is defined as follows:

$$\begin{aligned} \mathbf{R}_{c,k} &= \mathbf{H}_{c,c,k}\mathbf{Q}_{c,k}\mathbf{H}_{c,c,k}^H + \mathbf{R}_{\widehat{c,k}}, \\ \mathbf{R}_{\widehat{c,k}} &= \sum_{(j,i)\neq(c,k)} \mathbf{H}_{j,c,k}\mathbf{Q}_{j,i}\mathbf{H}_{j,c,k}^H + \sigma^2\mathbf{I}_N. \end{aligned} \tag{4}$$

This rate is strongly affected by intracellular interferences, especially when Rxs are placed at the cell's edge (Figure 1).

For example, the interference signals received in the DL may be very intense and even comparable to the signal strength for the user at the edge of the cell; this significantly reduces the achievable rate. To improve performance in cellular systems and maximize the weighted sum rate for all users, smart spatial signal processing techniques should be used in BSs and Rxs. Moreover, we consider the coordinated beam forming method, in which each BS sends data only to its users. However, the CSI is shared between the BSs for each BS to use more of its spatial dimensions to suppress interference generated in other cells (see Figure 2). Thus, we deal with an optimization problem, which is defined as follows:

$$\mathbf{G} = arg \max_{G} \sum_{c=1}^{C}\sum_{k=1}^{K} u_{c,k}k^T c, k, \tag{5}$$

where

$$s.t. tr\mathbf{G}_c\mathbf{G}_c^H \leq P_c \; for \; c \in C. \tag{6}$$

In the above relations, $\boldsymbol{G}$ is an abbreviation for $\{\mathbf{G}_c\}_{c\in C}$ and $u_{c,k} \geq 0$ is the weight of user k in cell c and is the issue utility function.

There are two algorithms to solve the above problem: the WSMSE algorithm and the KG algorithm; later, we describe them as follows.

3. WSMSE Algorithm

It is difficult to directly solve the optimization problem in (7) because it is extremely nonconcave in the G precoding matrix. To solve it, the linear filters of the receiver $\mathbf{F}_{c,k} \in \mathbb{C}^{N\times d_{c,k}}$, the error variance $\mathbf{E}_{c,k} \in \mathbb{C}^{d_{c,k}\times d_{c,k}}$ after linear filtering is received (given in (8)), and additional weighting matrices $\mathbf{W}_{c,k} \in \mathbb{C}^{d_{c,k}\times d_{c,k}}$ are considered to modify the utility function (7) and define the equation of optimization problem as follows [30]:

$$\begin{aligned} &\{\mathbf{G}, \mathbf{F}, \mathbf{W}\} = \\ &arg \min_{\mathbf{G},\mathbf{F},\mathbf{W}} \sum_{(c,k)} u_{c,k}\left(tr\left(\mathbf{W}_{c,k}\mathbf{E}_{c,k} - log\ de\ t\left(\mathbf{W}_{c,k}\right)\right)\right) \\ &s.t. tr\mathbf{G}_c\mathbf{G}_c^H \leq P_c \; for \; c \in C, \end{aligned} \tag{7}$$

along with

$$\mathbf{E}_{c,k} = E\left[\left(\mathbf{F}_{c,k}^H\mathbf{y}_{c,k} - \mathbf{s}_{c,k}\right)\left(\mathbf{F}_{c,k}^H\mathbf{y}_{c,k} - \mathbf{s}_{c,k}\right)^H\right]. \tag{8}$$

The above relation represents the mean squared error (MSE), i.e., the error variance in Rx. The advantage of defining the problem in this way is that the objective function is convex and depends on the second-degree G. We define $\rho_c = (P_c/\sigma^2)$ as the signal-to-noise ratio (SNR) in cell c. After using intermittent optimization techniques, the precoders are obtained from (8) as follows:

$$\mathbf{F}_{c,k} = \left(\sigma^2\mathbf{I}_N + \sum_{m=1}^{C}\sum_{l=1}^{K}\mathbf{H}_{m,c,k}\mathbf{G}_{m.l}\mathbf{G}_{m,l}^H\mathbf{H}_{m,c,k}^H\right)^{-1}\mathbf{H}_{c,c,k}\mathbf{G}_{c,k}, \tag{9}$$

$$\mathbf{W}_{c,k} = \left(\mathbf{I}_{d_{c,k}} - \mathbf{F}_{c,k}^H\mathbf{H}_{c,c,k}\mathbf{G}_{c,k}\right)^{-1}, \tag{10}$$

$$\mathbf{G}_{c,k} = \left(\sum_{J}^{C}\sum_{I}^{K} u_{j,i}\mathbf{H}_{c,j,i}^H\mathbf{D}_{j,i}\mathbf{H}_{c,j,i} + \lambda\mathbf{I}_M\right)^{-1}\mathbf{H}_{c,c,k}^H\mathbf{F}_{c,k}\mathbf{W}_{c,k}, \tag{11}$$

where $\mathbf{D}_{i,j} = \mathbf{F}_{i,j}\mathbf{W}_{i,j}\mathbf{F}_{i,j}$. Then, $\boldsymbol{F}_{c,k}$ and $\boldsymbol{W}_{c,k}$ are calculated; these two make new to $\boldsymbol{G}_{c,k}$ precedes. The Lagrangian λ_c must be adjusted by the bisection method to meet the power constraint conditions. However, if we disregard the bisector method, we can use Christensen et al. [31]; this reference provides a package term for Lagrange. Therefore, the work process is redefined as follows:

$$\mathbf{G}_{c,k} = \xi_c\left(\sum_{J}^{C}\sum_{I}^{K} u_{j,i}\mathbf{H}_{c,j,i}^H\mathbf{D}_{j,i}\mathbf{H}_{c,j,i} + \frac{tr\mathbf{D}_c}{M_{\rho c}}\mathbf{I}_M\right)^{-1}\mathbf{H}_{c,c,k}^H\mathbf{F}_{c,k}\mathbf{W}_{c,k}. \tag{12}$$

In (12), $\mathbf{W}_c = di\ ag(w_{c,1}, \ldots, w_{c,k})$, $\mathbf{A}_c = di\ ag(a_{c,1}, \ldots, a_{c,k})$, $\mathbf{D}_c = \mathbf{A}_c^H\mathbf{W}_c\mathbf{A}_c$, $\mathbf{A} = di\ ag(\mathbf{A}_1, \mathbf{A}_2, \ldots, \mathbf{A}_c)$, and

$\mathbf{D} = di\ ag(\mathbf{D}_1, \mathbf{D}, \ldots, \mathbf{D}_c)$, and ξ_c represents normalization and is defined as follows:

$$\xi_c^{(j)} = \sqrt{\frac{P_c}{\mathbf{G}_{c,k}\mathbf{G}_{c,k}^H}} = \sqrt{\frac{P_c}{\mathbf{\Psi}_c^{(j)}}}. \tag{13}$$

This process is repeated until it reaches the local optimum point.

4. KG Precoder Algorithm

Another method for solving the problem defined in (7) is to use the classical difference of the convex (DC) functions programming method described in the study by Kim and Giannakis [32, 36] and Al-Shatri and Weber [33]. The problem defined in (7) is due to the interference of a nonconvex problem. Therefore, in the KG algorithm, the desired signal is separated from a sum of rates of the remaining signals resulting in the problem being nonconvex. The rest of the signals are linearized using the Taylor expansion method because a linear function is both convex and concave. Put it simply, if we only consider the WSR dependence on $Q_{c,k}$, we can rewrite the objective function in (7) as follows:

$$\begin{aligned} WSR &= u_{c,k}\log\det\left(\mathbf{R}\frac{-1}{c,k}R_{c,k}\right) + WS\mathbf{R}\overline{c,k}, \\ WSR_{\widehat{c,k}} &= \sum_{(j,i)\neq(c,k)} u_{j,i}\log\det\left(\mathbf{R}\frac{-1}{j,i}\mathbf{R}_{j,i}\right). \end{aligned} \tag{14}$$

We consider first-degree Taylor series expansion in $\boldsymbol{Q}_{c,k}$ on $\widehat{\mathbf{Q}}$ *(i.e., all of* $\widehat{\mathbf{Q}}_{j,i}$*)* along with $\widehat{\mathbf{R}}_{j,i} = \mathbf{R}_{j,i}(\widehat{\mathbf{Q}})$; then,

$$WSR_{\widehat{c,k}}\left(\mathbf{Q}_{c,k},\widehat{\mathbf{Q}}\right) \approx WS\mathbf{R}_{\widehat{c,k}}\left(\widehat{\mathbf{Q}}_{c,k},\widehat{\mathbf{Q}}\right) - tr\left\{\left(\mathbf{Q}_{c,k}-\widehat{\mathbf{Q}}_{c,k}\right)\widehat{\mathbf{A}}_{c,k}\right\}, \tag{15}$$

with

$$\begin{aligned} \widehat{\mathbf{A}}_{c,k} &= \frac{\partial W\ S\mathbf{R}_{\widehat{c,k}}\left(\mathbf{Q}_{c,k},\widehat{\mathbf{Q}}\right)}{\partial\mathbf{Q}_{c,k}}\Big|_{\widehat{\mathbf{Q}}_{c,k},\widehat{\mathbf{Q}}} \\ &= \sum_{(j,i)\neq(c,k)} u_{j,i}\mathbf{H}_{c,j,i}^H\left(\widehat{\mathbf{R}}\frac{-1}{j,i} - \widehat{\mathbf{R}}_{j,i}^{-1}\right)\mathbf{H}_{c,j,i}. \end{aligned} \tag{16}$$

Note that the linearized expression for $WSR_{\widehat{c,k}}$ forms the lower limit for it. Now, setting aside the fixed expressions, we redefine the parameter $Q_{c,k} = G_{c,k}G_{c,k}^H$, to execute this linearization for all users, and complete the WSR cost function with constraint conditions; thus, we get Lagrangian as follows:

$$\begin{aligned} WSR(\mathbf{G},\widehat{\mathbf{G}},\lambda) = &\sum_{j=1}^{C}\lambda_c P_c + \sum_{c=1}^{C}\sum_{k=1}^{K} u_{c,k} log\,det\left(\mathbf{I}_{d_{c,k}} + \mathbf{G}_{c,k}^H\widehat{\mathbf{B}}_k\mathbf{G}_{c,k}\right) \\ &- tr\left\{\mathbf{G}_{c,k}^H\left(\widehat{\mathbf{A}}_{c,k} + \lambda_c\mathbf{I}_M\right)\mathbf{G}_{c,k}\right\}, \end{aligned} \tag{17}$$

where

$$\widehat{\mathbf{B}}_{c,k} = \mathbf{H}_{c,c,k}^H\widehat{\mathbf{R}}\frac{-1}{c,k}\mathbf{H}_{c,c,k}. \tag{18}$$

Indeed, the gradient of this convex low WSR bound (relative to $\boldsymbol{G}_{c,\,k}$) is still the same as the gradient according to the original WSR criteria. This allows us to consider it as a general condition of the eigenmatrix; thus, $\mathbf{G}_{c,k}^{'} = eigenmatrix(\widehat{\mathbf{B}}_{c,k}, \widehat{\mathbf{A}}_{c,k} + \lambda_c\mathbf{I}_M)$ is the generally normalized eigenmatrix of the above two matrices with eigenvalues $\sum_{c,k} = eigenmatrix(\widehat{\mathbf{B}}_{c,k}, \widehat{\mathbf{A}}_{c,k} + \lambda_c\mathbf{I}_M)$. The Lagrangian coefficients λ_c for all c are adjusted to meet the power limits $\sum_k \mathbf{P}_{c,k}(l,l) = P_c$. This can be done by performing the bisector method for each BS. Note that some Lagrangian coefficients may be zero. Assume $\sum_{c,k}^{(1)} \mathbf{G}_{c,k}^{'H}\widehat{\mathbf{B}}_{c,k}\mathbf{G}_{c,k}^{'}$ and $\sum_{c,k}^{(2)} = \mathbf{G}_{c,k}^{'h}\widehat{\mathbf{A}}_{c,k}$ $G_{c,k}^{'}$. The advantage of using (16) is that this equation allows direct power adaptation: by defining $\mathbf{P}_{c,k} \geq 0$ and substituting $\mathbf{G}_{c,k} = \mathbf{P}_{c,k}^{1/2}\mathbf{G}_{c,k}^{'}$ in (16), we get

$$\begin{aligned} WSR = &\sum_c \lambda_c P_c + \sum_{c,k}^{K}\left\{u_{c,k} log\ de\ t\left(\mathbf{I}_{d_{c,k}} + \mathbf{P}_{c,k}\sum_{c,k}^{(1)}\right)\right. \\ &\left. - tr\left(\mathbf{P}_{c,k} + \left(\sum_{c,k}^{(2)} + \lambda_c\mathbf{I}\right)\right)\right\}. \end{aligned} \tag{19}$$

This leads to water-filling with the knowledge of the following leakage:

$$\mathbf{P}_{c,k}(\mathrm{l},\mathrm{l}) = \left(\frac{1}{\sum_{c,k}^{(1)}(l,l)}\left(\frac{u_k}{\sum_{c,k}^{(2)}(l,l) + \lambda_c} - 1\right)\right)^{+}, \tag{20}$$

where for all l, we must have $\sum_{c,k}^{(1)} \geq 0$ (for all l s.t $\sum_{c,k}^{(1)} \geq 0$) where $z^{+} = max(0, z)$. Moreover, note that as with any intermittent optimization process (here too), there are many updates with different effects on convergence speed. The variables that need to be updated are $\mathbf{G}_{c,k}^{'}$, $\mathbf{P}_{c,k}$, and λ_c. The advantage of the DC method is that it works by using more or less specific values for many streams/user $d_{c,k}$ sequences. In other words, we can use the maximum number of eigenvalues $d_{c,k}^{max}$ of the eigenmatrix $\mathbf{G}_{c,k}^{'}$. Maximum eigenvalues are eigenvectors corresponding to the most considerable eigenvalues. The water-filling method automatically (in each iteration) determines how many stream sequences to maintain.

5. Deterministic Annealing Variant (DAV) and WSMSE-New

5.1. DAV. According to Negro et al. [34], one finds that the maximization problem in (7) is highly nonconvergent. At low SNRs (high noise variance), any interference is negligible compared to noise. Thus, all links can be considered decoupled. Therefore, rate maximization, like singleuser MIMO, becomes SNR maximization for the sequence to which total power is allocated. Optimal Tx and Rx filters are the left and single right vectors that correspond to the most considerable single channel value between Tx and Rx. This means that for SNR = 0, convergences to the global optimum are guaranteed.

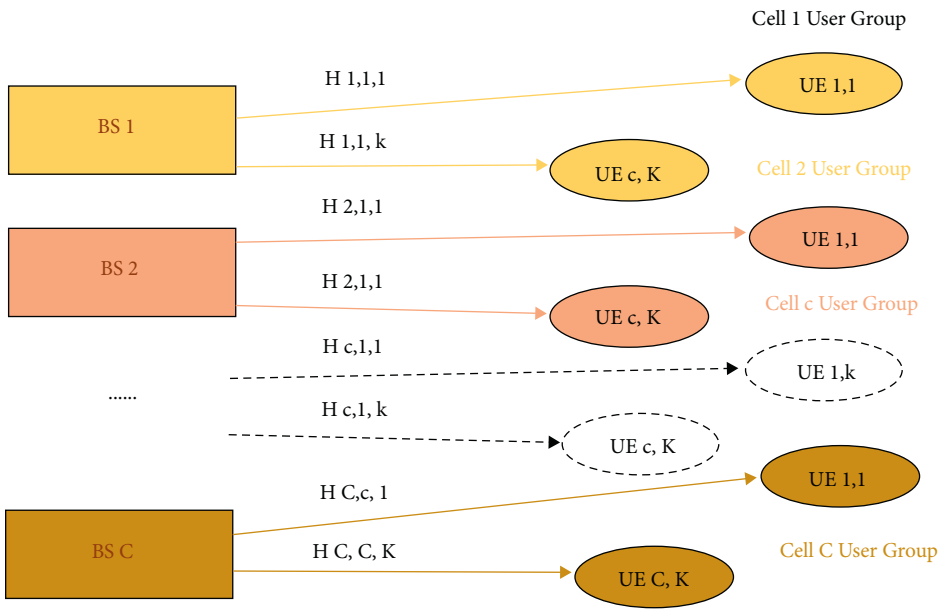

Figure 1: Interference broadcast channels or multicells, multiusers interference system model.

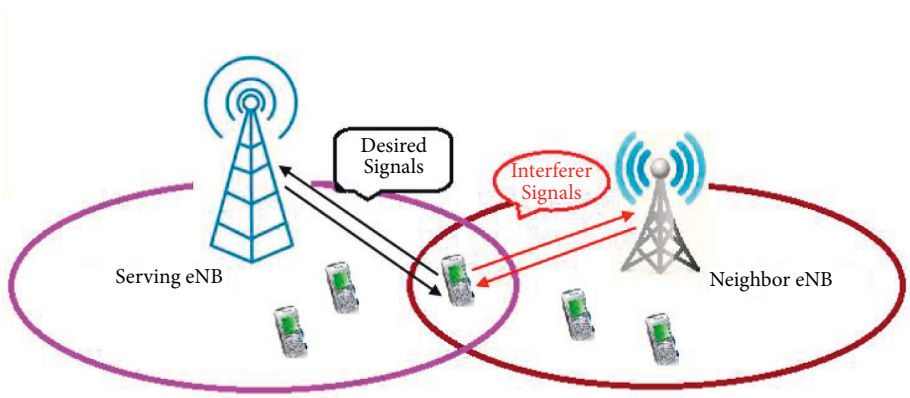

Figure 2: Intracell interference at the cell edges.

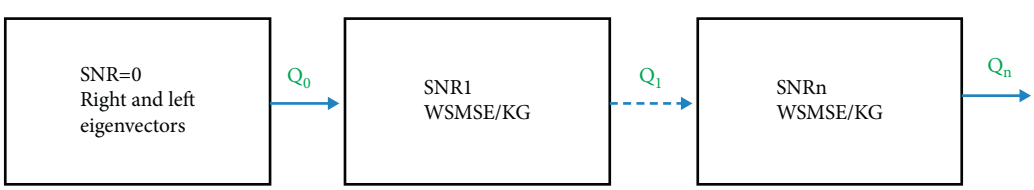

Figure 3: Deterministic annealing variant method.

Simultaneously, there are many more local optimum points because of the formation of additional sequences as soon as the SNR increases. Thus, as the SNR increases further, more local optimum sequences and points emerge. The idea of DAV (Figure 3) is to start the WSMSE (KG) with the response of the WSMSE (KG) algorithm at lower SNRs (starting from very low SNRs) that ensure convergence to the global optimum. This process goes on until a sequence distribution at higher SNRs is obtained that corresponds to the maximum sequence distribution for which the interference alignment is possible. Indeed, Tx and Rx filters reach the global response at very high SNRs.

To demonstrate the efficiency of the DAV method, we plot the total rate in terms of SNR for the IBC (Interference Broadcast Channels) system, for which the signals are pre-encoded by the WSMSE (KG) precursor and by the WSMSE (KG) precursor with the DAV. The last case means that the precursors at low SNR act as the trigger conditions for the precursor algorithm at high SNR. The classic WSMSE precoder is set up by eigenvectors to the right of the user

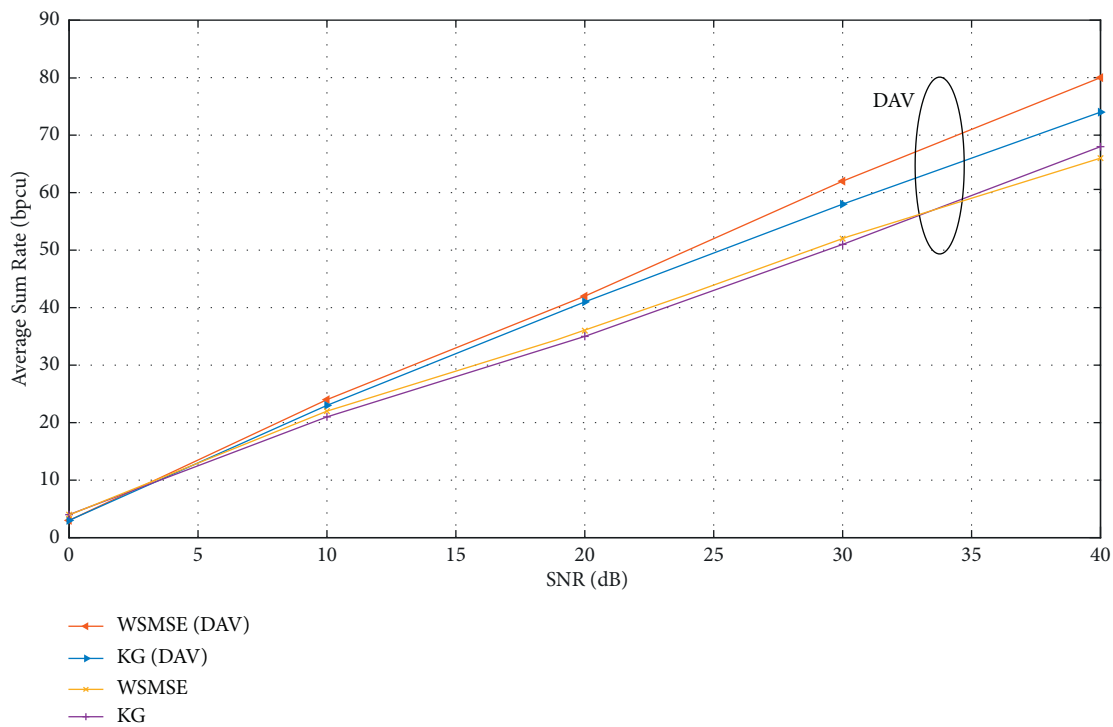

Figure 4: WSR in terms of SNR: $C = 5$, $K = 6$, $M = 5$, and $N = 5$.

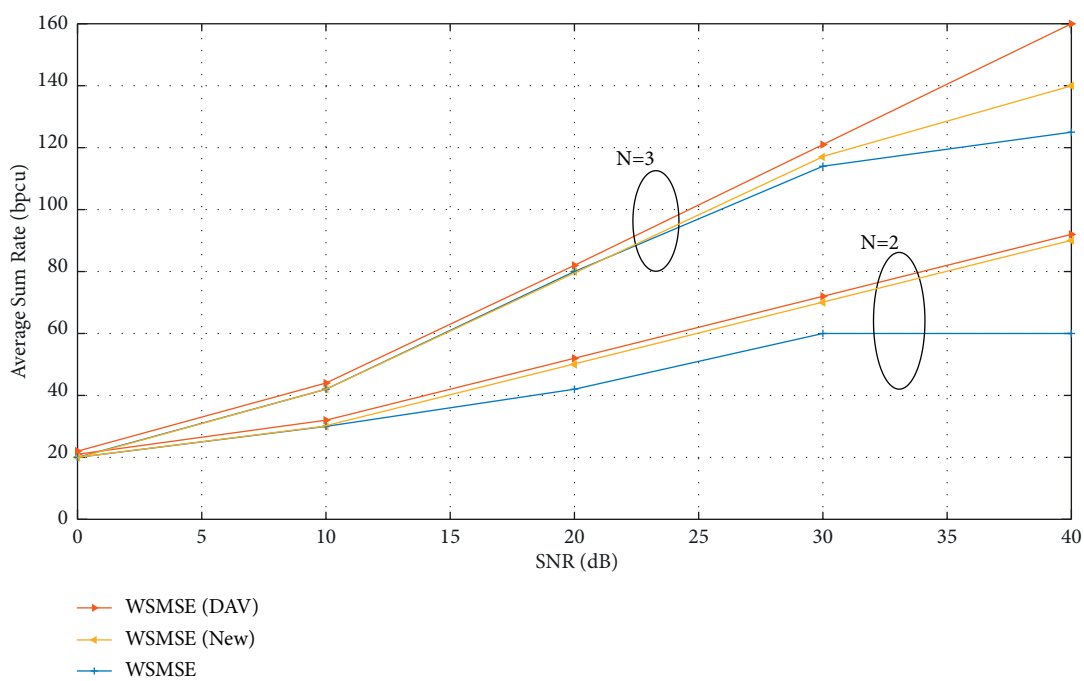

Figure 5: WSR in terms of SNR for $C = 5$, $K = 8$, $M = 15$, and $N = \{2, 3\}$.

channel. The classic KG is driven by zero matrices. The total number of iterations remains the same.

In other words, in using DAV, the number of iterations equals the total number of iterations needed to converge in each SNR used before the target SNR is reached. However, if we use classical algorithms, we will not need to iterate low SNRs, and we can run the algorithm immediately on the target SNR. Here, we will need some iterations equal to the total number of iterations if using DA. Figure 4 shows that DAV enhances the performance of the WSMSE and KG algorithms drastically.

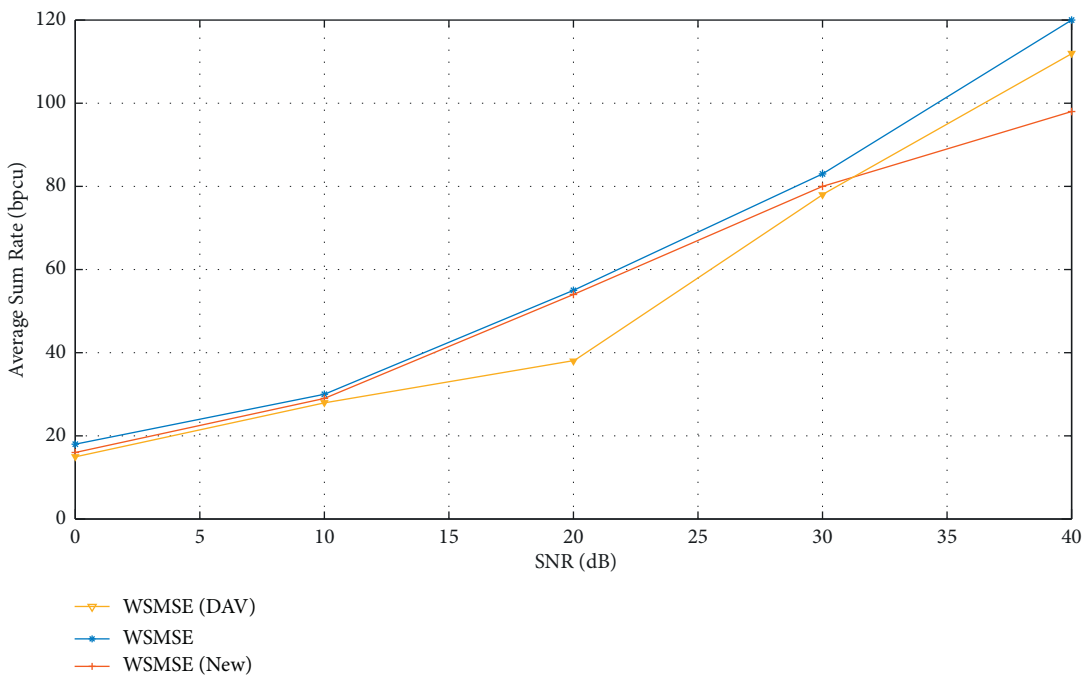

Figure 6: WSR in terms of SNR: $C = 3$, $K = 4$, $M = 10$, and $N = 2$.

Table 1: Simulation parameters and results of Figure 5.

$C = 5$	$K = 8$	$M = 15$	$N = 2$	$C = 5$ $K = 8$	$M = 15$	$N = 3$
SNR (dB)		WSR (bpcu)			WSR (bpcu)	
	New WSMSE	WSMSE	New WSMSE	New WSMSE	WSMSE	New WSMSE
0	20	20	20	20	20	20
5	26	26	26	32	32	32
10	37	37	37	45	45	45
15	42	39	42	62	62	62
20	53	42	53	80	42	80
25	62	50	62	99	97	100
30	76	60	76	117	115	120
35	82	60	82	129	120	140
40	92	60	92	139	125	158

5.2. WSMSE: A New Form. In this section, we present a novel version of WSMSE where the number of antennas is very large compared to the number of users; instead of Rx, MMSE (Minimum Mean Square Error), we use Rx matching filter (MF) as Rx user in detection (1). By using MF for DL detection in users, when the number of antennas at the BS is greater than the number of users, interuser interference will be suppressed [35]. Thus, in this case, we are no longer required to exchange the interference received by each user, and the Rx equation (10) becomes the following equation:

$$\mathbf{F}_{c,k} = \left(\sigma^2 \mathbf{I}_N + \mathbf{H}_{c,c,k}\mathbf{G}_{c,k}\mathbf{G}_{c,kl}^H\mathbf{H}_{c,c,k}^H\right)^{-1}\mathbf{H}_{c,c,k}\mathbf{G}_{c,k}. \quad (21)$$

This new developer can be named a WSMSE technique. This precoder's operation is as follows: Tx and Rx work together to eliminate incoming interference from sending to other users. If the number of Tx antennas is huge, Tx itself can eliminate the interference, and the complex Rx of the user is not required. Therefore, simple Rx techniques are optimized here.

The interesting point is that the new WSMSE precoder with a large number of Tx and simple Rx almost always achieves better local optimization points compared to the classical WSMSE precoder. The explanation is simple. If we use a simple Rx, the overlap will no longer create a link between Tx and Rx. This simplifies convergence. This does not affect performance as already stated since we have enough antennas in Tx to eliminate interference.

Figures 5 and 6 show the performance of the new WSMSE between the WSMSE and the WSMSE with the DAV, as the new WSMSE calls for fewer data to be exchanged and therefore achieves a better local optimum than the WSMSE. However, unlike WSMSE-DAV, it still cannot reach the global optimum. It has to be noted that, as shown in Figures 5 and 6, the method could only be used when the

Table 2: Simulation parameters and results of Figure 6.

$C = 3$	$K = 4$	$M = 10$	$N = 2$
SNR (dB)		WSR (bpcu)	
	New WSMSE	WSMSE	WSMSE (DAV)
0	17	17	17
5	20	22	22
10	22	35	35
15	26	44	44
20	39	59	59
25	58	69	72
30	80	80	89
35	97	87	103
40	112	97	118

number of Tx antennas is not less than the total number of receiving antennas of all users.

In sum,

(i) WSMSE with DAV is the extended version of WSMSE that uses DAV in the WSMSE precoder. Unlike WSMSE, which reaches the local optimum, this method achieves the global optimum.

(ii) The new WSMSE is a version of WSMSE where MF Rx replaces MMSE Rx. This method reaches better optimums than WSMSE and has a more straightforward Rx advantage. Thus, it requires less information exchange. Nonetheless, this method could only be used for many transmitter antennas.

(iii) The new WSMSE method is useful for analyzing large systems in MIMO single-string mode.

6. Conclusion

The results and parameters of our simulation are exposed in Tables 1 and 2.

In this section, we define the central problem, which is designing of precoders that maximize the weighted total rate for multicell scenarios under the condition of maximum power budget per cell. This rate is strongly affected by intracellular interference. We suggest using CBF. In CBF, all BSs exchange channel knowledge for the joint design of all BFs in the network. The problem is defined as the WSR maximization problem. If the ratio of the number of users served per cell is small enough to the number of transmitter antennas (approximately 1.10), simple linear beamformers like MF reaches great performance. In general cases, the two algorithms reach the best performance in terms of the total achievable rate. These two algorithms are WSMSE and KG. In the WSMSE algorithm, the problem of maximizing the total rate is solved by redefining it as the problem of minimizing the MSE function. The answer to this problem is obtained through an iterative algorithm. In this algorithm, we calculate $\boldsymbol{F}$, $\boldsymbol{W}$, and $\boldsymbol{G}$ alternately in each iteration. It has to be noted that $\boldsymbol{F}$ is for the filter on the Rx side, $\boldsymbol{W}$ is for the weight, and $\boldsymbol{G}$ is for the beam shaper. In the KG method, it is suggested that the objective function of the total rate should be divided into two functions, one function for the desired user rate *(c, k)* and the other function related to the total rate of the remaining users. These two functions are convex in $\boldsymbol{Q}_{c,k}$ (transmitter covariance) and nonconvex in $\boldsymbol{Q}_{c,k}$, respectively. It was suggested that the nonlinear part should be linearized to obtain a new objective function. This new function is the difference between a convex function and a linear function (a function that is both concave and convex). The answer to this new problem is obtained through the eigenmatrix of two matrices. This response is normalized; thus, the power must be adjusted. It is suggested that this be done using the water-filling approach. The WSMSE and KG both reach the local optimums. To force them to converge in global optimums, we must use the DAV method. Moreover, we suggest using the new WSMSE beam modulator. The new WSMSE is a version of the WSMSE algorithm obtained by substituting the **F** expression with the expression of MF in the MMSE. This beam generator is less complex compared to the WSMSE.

Advantages of the new WSMSE method are as follows:

(i) The new WSMSE calls for fewer data to be exchanged and, on the other hand, requires less information exchange

(ii) This method achieves better local optimums than the WSMSE

(iii) The new WSMSE method is useful for analyzing large systems in MIMO single-string mode

(iv) It is less complex compared to traditional WSMSE

Data Availability

Data are available. It will be shared at the request of the esteemed editor.

Conflicts of Interest

The authors declare that they have no conflicts of interest.

References

[1] E. Bjornson, J. Hoydis, M. Kountouris, and M. Debbah, "Massive MIMO systems with non-ideal hardware: energy efficiency, estimation and capacity limits," *IEEE Transactions on Information Theory*, vol. 60, no. 11, pp. 7112–7139, 2014.

[2] E. Bjornson, L. Sanguinetti, J. Hoydis, and M. Debbah, "Optimal design of energy-efficient multi-user MIMO systems: is Massive MIMO the answer?" *IEEE Transactions on Wireless Communications*, vol. 14, no. 6, pp. 3059–3075, 2015.

[3] E. G. Larsson, O. Edfors, F. Tufvesson, and T. L. Marzetta, "Massive MIMO for next generation wireless systems," *IEEE Communications Magazine*, vol. 26, p. 64, 2014.

[4] T. L. Marzetta, G. Caire, M. Debbah, I. Chih-Lin, and S. K. Mohammed, "Special issue on massive MIMO," *Journal of the Communications Network*, vol. 15, no. 4, pp. 333–337, 2013.

[5] H. Q. Ngo, E. G. Larsson, and T. L. Marzetta, "Energy and spectral efficiency of very large multiuser mimo systems," *IEEE Transactions on Communications*, vol. 61, no. 4, pp. 1436–1449, 2013.

[6] A. Pitarokoilis, E. Bj¨ornson, and E. G. Larsson, "ML detection in phase noise impaired SIMO channels with uplink

training," *IEEE Transactions on Communications*, vol. 64, no. 1, pp. 223–235, 2016.

[7] S. Yang and L. Hanzo, "Fifty years of MIMO detection: the road to large-scale MIMOs," *IEEE Communications Surveys & Tutorials*, vol. 17, no. 4, pp. 1941–1988, 2015.

[8] C. Qin, S. Zeng, C. Wang, D. Pan, W. Wang, and Y. Zhang, "A distributed interference alignment approach based on grouping in heterogeneous network," *IEEE Access*, vol. 6, pp. 2484–2495, 2018.

[9] A. Liu and V. Lau, "Hierarchical interference mitigation for Massive MIMO cellular networks," *IEEE Transactions on Signal Processing*, vol. 62, no. 18, pp. 4786–4797, 2014.

[10] A. F. Molisch, V. V. Ratnam, S. Han et al., "Hybrid beamforming for Massive MIMO – a survey," *IEEE Communications Magazine*, vol. 55, no. 9, pp. 134–141, 2017.

[11] H. Q. Ngo, E. G. Larsson, and T. L. Marzetta, "Massive mu-mimo downlink tdd systems with linear precoding and downlink pilots," in *Proceedings of the Fifty-first annual Allerton conference*, 02-04 October 2013.

[12] H. Q. Ngo, H. A. Suraweera, M. Matthaiou, and E. G. Larsson, "Multi-pair full-duplex relaying with massive arrays and linear processing," *IEEE Journal on Selected Areas in Communications*, vol. 32, no. 9, pp. 1721–1737, 2014.

[13] H. Q. Ngo, E. G. Larsson, and T. L. Marzetta, "Aspects of favorable propagation in massive MIMO," *European Signal Processing Conference (EUSIPCO)*, vol. 56, p. 897, 2014.

[14] H. Prabhu, J. Rodrigues, O. Edfors, and A. Fredrik, "Approximative matrix inverse computations for very-large MIMO and applications to linear precoding systems," in *Proceedings of the IEEE Wireless communications and networking conference (WCNC): PHY*, 07-10 April 2013.

[15] H. Wymeersch, N. Garcia, and D. T. M. Slock, "Optimal robust precoders for tracking the AoD and AoA of a mm-Wave path," *IEEE Transactions on Signal Processing*, vol. 66, no. 21, pp. 5718–5729, 2017.

[16] Y. Xu, G. Yue, N. Prasad, S. Rangarajan, and S. Mao, "User grouping and scheduling for large scale MIMO systems with two-stage precoding," in *Proceedings of the IEEE International conference on communications (ICC)*, 10-14 June 2014.

[17] M. Trick and B. Boukani, "Placement algorithms and logic on logic (LOL) 3D integration," *The Journal of Mathematics and Computer Science*, vol. 08, no. 02, pp. 128–136, 2014.

[18] A. Alkhateeb, G. Leus, and R. W. Heath, "Limited feedback hybrid precoding for Multi-User millimeter wave systems," *IEEE Transactions on Wireless Communications*, vol. 14, no. 11, pp. 6481–6494, 2015.

[19] O. E. Ayach, S. Rajagopal, S. Abu-Surra, Z. Pi, and R. W. Heath, "Spatially sparse precoding in millimeter wave MIMO systems," *IEEE Transactions on Wireless Communications*, vol. 13, no. 3, pp. 1499–1513, 2014.

[20] Z. Wang, M. Li, Q. Liu, and A. L. Swindlehurst, "Hybrid precoder and combiner design with low-resolution phase shifters in mmWave MIMO systems," *IEEE Journal of Selected Topics in Signal Processing*, vol. 12, no. 2, pp. 256–269, 2018.

[21] M. Trik, A. M. N. G. Molk, F. Ghasemi, and P. Pouryeganeh, "A hybrid selection strategy based on traffic analysis for improving performance in networks on chip," *Journal of Sensors*, pp. 1–19, 2022.

[22] W. M. Chan, T. Kim, H. Ghauch, and M. Bengtsson, "Subspace estimation and hybrid precoding for wideband millimeter-wave MIMO systems," in *Proceedings of the 50th Asilomar Conference on*, 06-09 November 2016.

[23] H. Lin, F. Gao, S. Jin, and G. Y. Li, "A new view of multi-user hybrid massive MIMO: non-orthogonal angle division multiple access," *IEEE Journal on Selected Areas in Communications*, vol. 35, no. 10, pp. 2268–2280, 2017.

[24] Y.-Y. Lee, C.-H. Wang, and Y.-H. Huang, "A hybrid RF/baseband precoding processor based on parallel-index-selection matrix-inversion bypass simultaneous orthogonal matching pursuit for millimeter wave MIMO systems," *IEEE Transactions on Signal Processing*, vol. 63, no. 2, pp. 305–317, 2015.

[25] V. Raghavan, S. Subramanian, J. Cezanne, A. Sampath, O. H. Koymen, and J. Li, "Single-user versus multi-user precoding for millimeter wave MIMO systems," *IEEE Journal on Selected Areas in Communications*, vol. 35, no. 6, pp. 1387–1401, 2017.

[26] M. Trik, S. Pour Mozafari, and A. M. Bidgoli, "An adaptive routing strategy to reduce energy consumption in network on chip," *Journal of Advances in Computer Research*, vol. 12, no. 3, pp. 1–12, 2021.

[27] D. Castanheira, P. Lopes, A. Silva, and A. Gameiro, "Hybrid beamforming designs for massive MIMO millimeter-wave heterogeneous systems," *IEEE Access*, vol. 5, pp. 21806–21817, 2017.

[28] J. Zhan and X. Dong, "Interference cancellation aided hybrid beamforming for mmWave multi-user massive MIMO systems," *IEEE Transactions on Vehicular Technology*, vol. 70, no. 3, pp. 2322–2336, 2021.

[29] S. Lavdas, P. K. Gkonis, Z. Zinonos, P. Trakadas, and L. Sarakis, "An adaptive hybrid beamforming approach for 5G-MIMO mmWave wireless cellular networks," *IEEE Access*, vol. 9, pp. 127767–127778, 2021.

[30] Q. Shi, M. Razaviyayn, Z. Q. Luo, C. He, and C. He, "An iteratively weighted mmse approach to distributed sum-utility maximization for a mimo interfering broadcast channel," *IEEE Transactions on Signal Processing*, vol. 59, no. 9, pp. 4331–4340, 2011.

[31] S. S. Christensen, R. Agarwal, E. de Carvalho, and J. M. Cioffi, "Weighted sum-rate maximization using weighted mmse for mimo-bc beamforming design," *IEEE Transactions on Wireless Communications*, vol. 7, no. 12, pp. 4792–4799, 2008.

[32] M. Trik, S. Pour Mozaffari, and A. M. Bidgoli, "Providing an adaptive routing along with a hybrid selection strategy to increase efficiency in NoC-based neuromorphic systems," *Computational Intelligence and Neuroscience*, vol. 2021, p. 8338903, 2021.

[33] H. Al-Shatri and T. Weber, "Achieving the maximum sum rate using d.c. programming in cellular networks," *IEEE Transactions on Signal Processing*, vol. 60, no. 3, pp. 1331–1341, 2012.

[34] F. Negro, I. Ghauri, and D. T. M. Slock, "Deterministic annealing design and analysis of the noisy mimo interference channel," in *Proceedings of the IEEE Information theory and applications (ITA) Workshop*, 06-11 February 2011.

[35] L. Lu, G. Y. Li, A. L. Swindlehurst, A. Ashikhmin, and R. Zhang, "An overview of massive MIMO: benefits and challenges," *IEEE journal of selected topics in signal processing*, vol. 8, no. 5, pp. 742–758, 2014.

[36] S.-J. Kim and G. B. Giannakis, "Optimal resource allocation for mimo ad hoc cognitive radio networks," *IEEE Transactions on Information Theory*, vol. 57, no. 5, pp. 3117–3131, 2011.

[37] A. Alameer Ahmad, H. Dahrouj, A. Chaaban, A. Sezgin, and M. S. Alouini, "Interference mitigation via rate-splitting and common message decoding in Cloud radio access networks," *IEEE Access*, vol. 7, pp. 80350–80365, 2019.

[38] W. Ni and X. Dong, "Hybrid block diagonalization for massive multiuser MIMO systems," *IEEE Transactions on Communications*, vol. 64, no. 1, pp. 201–211, 2016.

Hindawi
International Journal of Antennas and Propagation
Volume 2022, Article ID 5883490, 10 pages
https://doi.org/10.1155/2022/5883490

Research Article

A Novel Model for Calculating Uplink-Downlink Spectral Efficiency in Cooperative Communication MIMO Systems

Mohammad Reza Pouryeganeh, Azim Fard, and Mohammad Bagher Tavakoli

Department of Electrical Engineering, Islamic Azad University, Arak, Iran

Correspondence should be addressed to Azim Fard; azimfard@cra.ir

Received 9 January 2022; Revised 23 April 2022; Accepted 15 May 2022; Published 28 June 2022

Academic Editor: Sami Myllymäki

Cooperative communication that enables the use of relays between a base station (BS) and end users is an effective technique against fading to improve network performance, especially in increasing spectral efficiency (SE) and network coverage. However, systems that use cooperative communication have weaknesses in the structure, such as resistance to latency and an increase in the bandwidth of substitute users (SU), which can be improved by optimizing the relay selection method effectively. The system due to insufficient spacing between antennas and insufficient scattering in the channel has spatially faded that leads to spatial correlation. We use Kronecker statistical model correlated multiantenna channels to implement detection techniques and eliminate interference in cooperative communication. The validity of the Kronecker model lies in the fact that correlation coefficients of transmission are independent of the receiving antennas. In other words, the spatial correlation model separates both ends of the communication link. Therefore, using the minimum mean-squared-error (MMSE) technique, we have removed the need for optimal elimination of interference between SU and relay service provider or primary user (PU). Regardless of BS performance, the scope of this work is restricted to the layer after the BS in the interaction between the service providers and substitute users. The primary purpose of the presented method is to improve the spectral gain through the elimination of interference. Simulation results show about 10% of SE improvement along with considerable traffic gain.

1. Introduction

Point-to-point MIMO systems refer to communicating two multiple antennas devices with each other; in this case, for two terminals of link, multiantenna equipment is needed, increasing the cost of systems. Multiuser MIMO with single-antenna users is used, and multiplexing gain can be shared by all users. For the purpose of more enhancement in reliability, spectral and energy efficiency, and relatively simple processing in cellular wireless networks, massive multiple-input multiple-output (Massive MIMO) systems are used, which the base stations (BSs) equip with very large numbers of antennas; therefore, complexity and cost will be increased. Instead of that, a cooperative MIMO can be used as multiple devices group into virtual antenna arrays (VAAs). Within a VAA and between possibly different VAAs, multiple point-to-point links can exist; therefore, cooperative MIMO improves capacity, cell edge throughput, and coverage, although these systems have high complications and extensive signaling for forming cooperative devices. Three strategies used for relay-based MIMO include amplify-and-forward, decode-and-forward, and compress-and-forward techniques.

Relay networks have a good advantage in terms of energy savings and are mainly achieved by a short transmission range that reduces path loss and decreases transmission power. The amount of energy-saving is related to how the relay is selected. Considering the coordination overhead, as the number of cooperators increases, the energy efficiency of cooperative communication may decrease [1].

This issue is of particular importance in the fifth generation of cellular wireless communications, especially in the mmWave frequency range. Based on the nature of this frequency range and the lesser number of reflections, areas

without coverage will gradually increase. Therefore, the use of tools and coverage improvement techniques is particularly important. Relay operations manage according to various criteria, for example, maximum SNR, best harmonic mean, nearest neighbor selection, and difference-based selection. Hybrid methods could be implemented by a combination of the above methods. In this regard, we have referred to the clustering of users in the peripheral environment of a relay user, located at the head of end users. Figure 1 shows the PUs in the head of clusters.

Kronecker model, also known as correlated multiple-input multiple-output (MIMO) channels, has theoretically been studied mainly in the context of the separator correlation model [2, 3], and the virtual representation framework for uniform linear arrays (ULAs) [4–7]. Spatial correlation is determined by the transfer of weights (complex excitation of the Tx array elements), direction, and polarization of the irradiated power. Transferred weights determine which elements of the array antenna will be activated and how their transmitted power would be managed for radiation. For example, radiation in specific directions may only activate some elements and leave others inactive, which affects the spatial correlation in the Rx array. This model provides accurate results for MIMO modeling in specific settings for the small number of antenna elements. However, several studies have been conducted on how different detectors are applied in cooperative communication in the fifth generation (5G) and heterogeneous networks [8]. Furthermore, the incorporation of the Kronecker model and virtual channel representation models can alleviate the effect of the joint correlation structure of the channel to enhance spectral efficiency [9, 10].

Many researchers have focused on the design of low-complexity detection algorithms for the generalized spatial modulation (GSM) system, for example, the compressive sensing (CS) [11–14], the ordered block (OB) MMSE [15, 16], the message passing [17], the Gaussian approximation [18, 19], and sphere decoding (SD) [8, 20, 21]. Dytso et al. [22] considered a Gaussian channel with one transmitter and two receivers in which the maximization of the input-output mutual information at the primary/intended receiver is subject to a disturbance constraint measured by the MMSE at the secondary/unintended receiver and derived new upper bounds on the input-output mutual information of this channel that held for vector inputs of any length. Some authors, such as Imam et al. [23], addressed interference cancellation in uplink multiuser (MU) MIMO system with an amplify and forward (AF) full-duplex (FD) relay, and an equivalent relay model is adopted to suppress the self-interference. Moreover, block diagonalization (BD) is applied to design postprocessor filters to null the MU interference and extract the direct and relayed links signals for performing the MMSE combination of the extracted signals. In [24, 25], the author uses two protocols and combines them with multiantenna users and MMSE-SIC detection in a downlink; the system can achieve an optimal spectral efficiency (SE) and suboptimal SE performance regardless of a number of the users in the system [26]. The performance of an uplink large-scale MIMO system with an MMSE-SIC detector is studied. In [27] particular, considers the coherent detection MIMO-MMSE-SIC of M-PSK signals in a flat Rayleigh fading environment, where after serial-to-parallel conversion, several substreams of symbols are simultaneously transmitted by using an antenna array, thereby increasing the spectral efficiency.

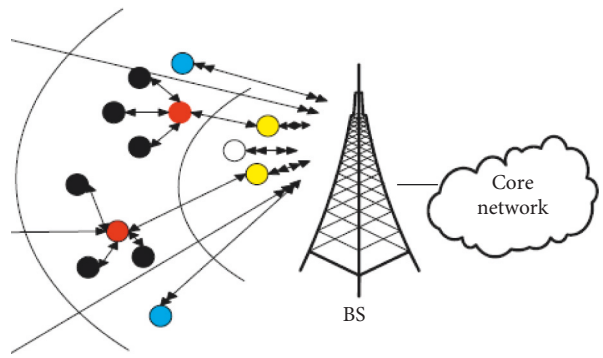

Figure 1: Head cluster users (red points: primary users and black points: secondary users).

As seen in most of these works, the combining vector method has been used to detect exchange channels between users and service providers. Due to the accuracy and importance of MMSE-based methods, it has higher efficiency and validity than other methods such as MR and ZF; still, MMSE-based matrix calculations are more complex and repetitive than other methods.

In the first section, we model the cooperative communication MIMO system with the central base station and coherence blocks for primary-relay users, and secondary users then achieve MMSE of the channel response based on the Kronecker statistical channel model. In step 3, we calculate the cooperative user's achievable SE in the uplink. We suppose PU is aware of the statistical information about the CSI of SUs. Linear MMSE detector by separating the independent string NK uses to maximize uplink SE of special string from user k. In Section 4, we calculate the achievable SE of cooperative users in the downlink receiver signal with the assumption the users do not have any instant CSI from BS and based on only the covariance channel matrix. Figures describe more details. Finally, we summarize our results in section 5.

2. System Model

Consider a time division duplex (TDD) MIMO system equipped with PU with antennas and K secondary users (SU) having N antennas (Figure 2). In this model, PUs act as relays between the K number of SUs and one BS. Assume that each coherence block (CB) contains S symbols, and each user in each CB remains unchanged. We consider N_r and N_t as numbers of receiver antennas and transmitter antennas, respectively. Then, the channel response of user k and PU relay is $H\varepsilon\mathbb{C}^{N_r\times N_t}$. The fading phenomenon is considered spatially fading due to the small distance of antenna elements and low channel scattering. In this model, we use the canonical Kronecker form to describe spatial correlation.

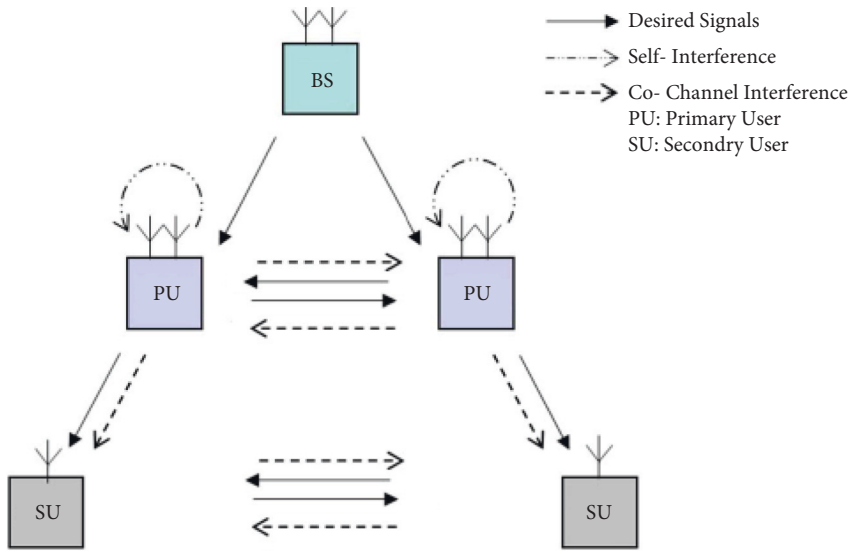

Figure 2: Schematic of the system model for downlink.

The Kronecker model has mainly developed for Rayleigh distributed channels having identically distributed (i.i.d.) zero-mean circularly symmetric complex Gaussian distributions. This model indicates a correlation on spatial diversity R_{MIMO} due to proximity antenna [7, 28, 29].

$$R_{Rx} = \frac{1}{Nr}\mathbb{E}\left[\mathrm{HH}^T\right], \qquad R_{Tx} = \frac{1}{Nt}\mathbb{E}\left[H^T H\right], \tag{1}$$

$$R_{\mathrm{MIMO}} = R_{Tx} \otimes R_{Rx}, \tag{2}$$

where H, $\mathbb{E}[\cdot]$, R_{Rx}, and R_{Tx} are channel responses, expected value, receiver correlation, and transmitter correlation, respectively.

In uplink communication, Nr is the number of the receiver PU antenna elements M, and Nt is the number of the transmitter SU antenna elements N. In (2), "⊗" represents the multiplier of Kronecker. In other words, the correlation is between the transmitter and receiver elements. After applying the operator ⊗ in (2), we will have the channel response of the whole system in the form of (3) [30]. We consider a downlink in a wireless narrowband system based on Rayleigh fading MIMO by considering a relay transmitter with N_t antennas and users with the N_r antennas. The model assumes that the statistical nature of the separation exists and is presented according to the classical Kronecker model as follows [31]:

$$H_k = R_{r,k}^{(1/2)} H_{i.i.d} R_{t,k}^{(1/2)}, \tag{3}$$

where $R_{t,k} \in \mathbb{C}^{N_t * N_t}$ represents the spatial correlation matrix in user k and $R_{r,k} \in \mathbb{C}^{N_r * N_r}$ represents the spatial correlation matrix in PU for the link of the k_{th} user. The large-scale fading parameter exists in $R_{r,k}$ and can be considered as $(1/M)tr(R_{r,k})$ that tr(.) is the trace of a non-negative self-adjoint operator and shows the sum of elements on the main diagonal (the trace of a matrix is the sum of its eigenvalues, and it is invariant with concerning a change of basis).

We consider the $R_{t,k}$ based on eigenvalues, so $R_{t,k} = U_k \Gamma_k U_k^H$ in this expression $U_k \in \mathscr{C}^{N_t \times N_t}$ is a unitary matrix, and $\Gamma_k = \mathrm{diag}\{\mu_{k,1}, \ldots, \mu_{k,N_t}\}$ is eigenvalues.

To estimate all PU MIMO channels in the uplink, the $T = N * K$ number of orthogonal pilot signals are required. $F_k \in \mathbb{C}^{N_t * K}$ represents the pilot sequence signal in the uplink. Assuming that each PU is aware of only the channel state information (CSI) value of each user's CSI, this includes the PU concerning BS [30, 32, 33], which is out of our debate, and we merely model the communication between PU and SU. In this case, based on the nature of using the Kronecker model and the need to minimize the value of MMSE in the channel approximation, $tr(F_k F_k^H) \leq \mathrm{TP}_k$ where $F_k = U_k L_k^{(1/2)} V_k^T$ and P_k is the maximum power level of the transmitter. The maximum number of users is K, and $L_k = \mathrm{diag}\{L_{k,1}, \ldots, L_{k,N_t}\}$ is the power distribution on the N_t channel, which is on the diameter of the matrix L, and $V_k \in \mathbb{C}^{T * N_t}$ with the condition $V_k^H V_k = \mathrm{TI}_{N_t}$ and based on the orthogonality, if $k \neq l$, then $V_k^H V_l = 0 k \neq l$. Because other PUs should not interfere with each other, and at any time, a user cluster containing k number of users interacts with only one PU. In this case, the received signal in the PU, Y, will be as follows [34]:

$$Y = \sum_{k=1}^{K} H_k F_k + n = \sum_{k=1}^{K} G_k D_k^{1/2} V_k^T + n, \quad Y \in \mathbb{C}^{N_r \times T}, \tag{4}$$

where n is additive Gaussian noise; we define the matrices G_K, D_K as $G_k = R_{r,k}^{1/3} H_{i.i.d} U_{t,k}, D_k = \Gamma_k L_k$ for use in matrix operations. In this case, the amount of received noise has been considered as vec(n) and $\mathrm{vec}(n) \sim CN(0, \sigma^2 I_{\mathrm{TM}})$, where $\sigma^2 I_{\mathrm{TM}}$ denotes additive receive noise and $\mathrm{vec}(\cdot)$ is the

vectorization operator; the vec operator is an operator that transforms a matrix into a column vector by vertically stacking the columns of the matrix. In addition, it assumes that PU is aware of statistical information related to D_k [30], and by referring to this, the MMSE approximation of $\hat{g} = \mathrm{vec}(G_k)$ can be formulated:

$$\hat{g}_k = \left(D_k^{(1/2)} \otimes R_{r,k}\right)\left\{\left(D_k \otimes R_{r,k}\right) + \frac{\sigma^2}{T} I_{\mathrm{MN}}\right\}^{-1} b_k. \quad (5)$$

By use of (5), the value of the $\hat{G}$ channel response could be calculated, and by using MMSE, the difference with the channel response H could be minimized. This equation $b_k = \mathrm{vec}((1/T)Y_k V_k^*) = \mathrm{vec}(G_k D_k^{(1/2)} + (1/\sqrt{T})nV_k^*)$ and the expression $(\sigma^2/T)I_{\mathrm{MN}}$ denote Gaussian noise with zero mean and variance σ^2, respectively. Orthogonally, the mathematical expectation $\hat{g}_{k,i}\hat{g}_{k,j}^H$ is calculated as follows:

$$\mathbb{E}\left\{\hat{g}_{k,i}\hat{g}_{k,j}^H\right\} = \begin{cases} \Phi_{k,i}, & i = j, \\ 0, & i \neq j, \end{cases} \quad (6)$$

where $\Phi_{k,i}$ is the MMSE of the channel response between PU and k^{th} SU as the client and $\Phi_{k,i}$ is equal to $\Phi_{k,i} = d_{k,i}R_{r,k}(d_{k,i}R_{r,k} + (\sigma^2/T)I_M)^{-1}R_{r,k}$. With this amount as vector combining, we examine the spectral efficiency in uplink and downlink between PU and SU.

3. Cooperative Users Achievable SE in Uplink

Consider the system as a multiple access MIMO channel. If the received signal Y in the service user is equal to

$$Y = \sum_{k=1}^{K} G_k F_k' S_k + n, \quad (7)$$

where S is the information vector of the symbols sent from SU to PU, $S_k \in CN(0, I_N)$, and $n \in CN(0, \sigma^2 I_M)$. Matrices S, G, when the PU is mindful of the perfect CSI of SU, i.e., each transmitter is cognizant of its CSI. In total, the PU is aware of the statistical information about the CSI of SUs so that the precoding matrix can be formed with the eigenvector [30, 34].

So we can get the precoding matrix. In this case, each transmitter in the PU has only its own statistical CSI, the precoding directions of each user that maximizes the total capacity with its particular spatial correlation matrix vectors. This assumption is expressed like double scattering and is consistent with the prevailing reality based on the results [35, 36].

We assume that the receiver has imperfect CSI, while each transmitter only has access to its own statistical CSI. Consider the matrix F_k, $k = 1, \ldots K$, as the precoding of the user matrix in the uplink, where $F_k' = U_k P_k^{1/2}$, P_k is a diagonal matrix in the form: $P_k = \mathrm{diag}\{p_{k,1}, \ldots, p_{k,N}\}$, and $F_k' \in C^{N\times N}$. Therefore, (7) has been rewritten as follow based on the matrix of eigenvalues:

$$Y = \sum_{k=1}^{K} H_k F_k' S_k + n = \sum_{k=1}^{K} G_k \Gamma_k^{1/2} P_k^{1/2} S_k + n_k. \quad (8)$$

Now, if we consider the mutual information between S and Y as a conditional probability and $S = [s_1, \ldots, s_k]$ and the channel response estimated under imperfect CSI in (5), then the conditional probability governing the relation (9) will be

$$\begin{aligned} I(Y, \hat{G}; S) &\geq \sum_{k=1}^{K} \mathbb{E}\left\{\log_2\left|I_N + Q_k \hat{G}_k^H \sum_k \hat{G}_k\right|\right\} \cong \sum_{k=1}^{K} R_{ul,k}^{sic}, \\ Q_k &= \Gamma_k P_k \sum_k \\ &= \left(\sum_{l\neq k} \hat{G}_l Q_l \hat{G}_l^H + Z + \sigma^2 I_M\right)^{-1}, \\ Z &= \sum_{l=1}^{K}\sum_{n=1}^{N} \lambda_{l,n} p_{l,n}\left(R_{r,l} - \Phi_{l,n}\right). \end{aligned} \quad (9)$$

In (9), the changes of the average channel compared to the approximation of the channel are calculated, where $\prime\prime|\cdot|\prime\prime$ represents the matrix determinant and N is the number of exchange strings between PU and SUs.

In (9), the lower bound signal capacity using the MMSE-SIC detector can be described as achievable SE for k_{th} primary user (PU) based on information theory with the condition of uncorrelated Gaussian couser interference.

For example, from the user k, the signal of S_k strings in the form of imperfect CSI, uncorrelated Gaussian signal is received through the channel with imperfect CSI $\hat{G}_k Q_k^{(1/2)}$. This signal passes through the factor $n_k = Y - \hat{G}_k Q_k^{1/2} S_k$ is broken as an uncorrelated interference factor that has the covariance of the matrix $(\sum_k)^{-1}$, in which by applying the MMSE-SIC procedure to the S_k strings, the value of SE is ergodic, based on the (9). Equation (9) is the general form of achievable SE [37, 38] in MIMO systems.

When the SIC procedure is computable, the number of N stream data can be transferred to SU_k and now can use the linear MMSE detector to separate the independent string NK. Based on [39], a linear MMSE detector can maximize uplink SE for the i_{th} string for k_{th} user as $f_{k,i} = \sqrt{\lambda_{k,i} p_{k,i}} \sum \hat{g}_{k,i}$. Linear detector application $f_{k,i}$ to the signal in (7) causes an achievable SE for user k as follows:

$$R_{\mathrm{UL},k}^{\mathrm{MMSE}} = \sum_{i=1}^{N} \mathbb{E}\left\{\log_2\left(1 + \mathrm{SINR}_{k,i}^{\mathrm{UL}}\right)\right\}. \quad (10)$$

SINR value of the i_{th} string in (10) is equal to

$$\mathrm{SINR}_{k,i}^{\mathrm{UL}} = \frac{\lambda_{k,i} p_{k,i}\left|f_{k,i}^H \hat{g}_{k,i}\right|^2}{\mathbb{E}\left\{f_{k,i}^H\left(\mathrm{YY}^H - \lambda_{k,i} p_{k,i} \hat{g}_{k,i}\hat{g}_{k,i}^H\right) f_{k,i} | \hat{G}\right\}}. \quad (11)$$

It seems that the condition of: $R_{\mathrm{UL},k}^{\mathrm{MMSE}} \leq R_{\mathrm{UL},k}^{\mathrm{SIC}}$ is required to effectively eliminate user string interference via $f_{k,i}$; see Appendix A for (11).

4. Achievable SE of Cooperative Users in Downlink

For simplicity, we assume that CSI feedback from the reference BS does not reach the SU. Of course, this is a common assumption in MIMO because we have not considered any CSI improvement strategy and only consider cooperative communication via PU. In addition, by using CSI feedback, only 25% of users through could be improved cooperative communication. Therefore, in this case, users do not have any instant CSI, and our reference, in this case, is only the covariance form in the form $\overline{G}_k \cong \Gamma_k^{(1/2)}\mathbb{E}\{G_k^H W_k\}\Omega_l^{(1/2)}$ to know that the effective average will be the channel response, where $W_k \in \mathscr{C}^{N_t \times N_r}$ is the downlink precoding matrix of user k and $\Omega_k = \mathrm{diag}\{w_{k,i}, \ldots, w_{k,N_r}\}$ indicates the add-on power for N stream for users. The total power of SU is equal to P_k, and the signal received in SU is equivalent to

$$Y = H_k^H \sum_{l=1}^{K} W_l \Omega_l^{(1/2)} S_l + n_k \in \mathscr{C}^{N\times 1}, \tag{12}$$

where $S_l \sim NC(0, I_M)$ are desired signals for the end user l and the $n_k \sim CN(0, \sigma^2 I_N)$ the received added noise. Without losing the generality of the work, consider that user k uses the eigenvalue matrix of its correlation matrix, U_k^H. For detection in the first step of channel correlation matching, the received signal Z_k is equal to

$$\begin{aligned} Z_k &= U_k^H Y_k \\ &= \Gamma_K^{(1/2)} H_k^H \sum_{l=1}^{K} W_l \Omega_l^{(1/2)} S_l + U_k^H n_k. \end{aligned} \tag{13}$$

In (13), we need to calculate the lower bound mutual information between Z_k, S_k, that is, $I = (Z_k; S_k)$, to calculate the minimum channel capacity to join SE.

According to the definition of mutual information based on entropy:

$$I(Z_k; S_k) = h(S_k) - h(S_k Z_k). \tag{14}$$

If $S_k \sim NC(0, I_N)$, then $h\ (S_k) = \log_2|\pi e I_N|$. However, by applying MMSE to S_k value:

$$\hat{S}_k = \overline{G}_k^H \left[\Gamma_k^{(1/2)}\mathbb{E}\left\{G_k^H \sum_{l=1}^{K} W_l W_l^H \Omega_l\right\}\Gamma_k^{(1/2)} + \sigma^2 I_N\right]^{-1} Z_k. \tag{15}$$

Now we calculate $\tilde{S}_k = S_k - \hat{S}_k$ as the error estimate S_k concerning $h(S_k|Z_k)$, the entropy of the upper bound of the Gaussian vector with zero mean, which is the covariance matrix, is as follows:

$$h(S_k|Z_k) \le \log_2|\pi e \mathbb{E}|\left\{\tilde{S}_k \tilde{S}_k^H\right\} = \log_2\left|\pi e\left(I_N - \overline{G}_k^H A_k \overline{G}_k\right)\right|. \tag{16}$$

And $\mathbb{E}\{\cdot\}$ is the expectation of the stochastic channel realizations. In (14), by placing the equations, we have the values of $h(S_k)$ and $h(S_k Z_k)$:

$$I(Z_k; S_k) \ge \log_2\left|I_N + \overline{G}_k^H \overline{A}_k \overline{G}_k\right| \approx R_{\mathrm{DL},k}^{\mathrm{SIC}}, \tag{17}$$

$$Z_k S_k \overline{A}_k \overline{A}_k = \left(\left[\Gamma_k^{(1/2)}\mathbb{E}\left\{G_k^H \sum_{l=1}^{K} W_1 W_1^H \Omega_1\right\}\Gamma_k^{(1/2)} + \sigma^2 I\right] - G_k \overline{G}_k^H\right)^{-1}. \tag{18}$$

Equation (17) shows mutual information between $Z_{k,}$ and S_k. In addition, in (13), the MMSE estimate has been applied to the received signal; in this case, the combination vector (CV), $\mathrm{CV}_{k,i}$, will be equal to

$$CV_{\mathrm{k,i}} = A_k g_{k,i}, \tag{19}$$

where the CV vector represents the combining vector (g) and $\overline{g}_{k,i}$ represents the $i^{\mathrm{th}} i_{th}$ column of the $\overline{G}_k$ matrix. Knowing $\overline{G}_k$, we can apply the MMSE estimate for the i_{th} string to the downlink and obtain the SE value with the MMSE linear estimate, which in (18) is equal to $A_k = \overline{A}_k^{-1} + G\overline{G}_k^H$. By applying this approximation, the value of user SE downlink k is equivalent to

$$R_{dl,k}^{\mathrm{MMSE}} = \sum_{i=1}^{N} \mathbb{E}\left\{\log_2\left(1 + \mathrm{SINR}_{k,i}^{dl}\right)\right\}. \tag{20}$$

The SINR value of user k in the downlink could be calculated by (21):

$$\mathrm{SINR}_{k,i}^{dl} = \frac{\left|r_{k,i}^H \overline{g}_{k,i}\right|^2}{r_{k,i}^r \mathbb{E}\left\{Z_k Z_k^H\right\} r_{k,i} - \left|r_{k,i}^H \overline{g}_{k,i}\right|^2}. \tag{21}$$

The MMSE-SIC detector performs better than the MMSE detector in the downlink. To compare the MMSE-SIC and linear MMSE method's performance in a cooperative communication system, we extract uplink and downlink SE diagrams in this system.

5. Channel State Information (CSI)

First, the channel should be estimated in real wireless systems. Then this estimated channel will be used in forward

and reverse links. If the estimation has a difference with the exact channel, the channel information, named imperfect CSI, can be modeled by means of a Gauss–Markov uncertainty of the form:

$$G_W = \sqrt{1 - \beta^2 \hat{G}_W} + \beta n, \tag{22}$$

where $G_W \in\in CN$ (0, I) is the true Gaussian part of the channel matrix, $\hat{G}_W \in\in CN$ (0, I) is the imperfect observation of G_W available to the nodes, and $n \in\in CN$ (0, I) is an i.i.d. Gaussian noise. Partial CSI characterizes β has values of $0 < \beta < 1$ for partial CSI when $\beta = 0$ we have perfect CS and $\beta = 1$ corresponds to no CSI knowledge. β is a function of different system parameters. Using MMSE channel estimation, β is a function of pilot symbol SNR [40].

Supposing β equals zero, so using perfect channel knowledge leads to

(1) Have all certain CSI for optimal signal detection

(2) Do not have any decrease in SINR related to CSI

Using $\beta = 1$ and partial channel knowledge cause to

(1) Have no particular detection signal

(2) Have reduced SINR

In this work, we use MMSE-SIC, so the pilot symbols affect β. The number of needed pilot sequences is related to the number of all K users, number of N user antennas, and number of M PU antennas; if pilot sequences increase more than expected, preserving the orthogonality will be hard that would lead to pilot contamination. Our PUs have imperfect CSI. In actual work, by changing and settling N, M, and K, we can have semiperfect CSI. But, when the number of cells is considered additionally, more increase in cellular network dimension aggravates pilot contamination; also, in this case, reducing other parameters can diminish it.

Figure 3 shows the SE values for uplink and downlink using the MMSE-SIC and linear MMSE methods, which are plotted for the estimated solution and the simulated result. These values have been plotted for the incremental range of the number of cooperative user antennas or PU antennas and the number of exchanged strings $N = 1$ and $N = 3$, respectively, where the number of users is $K = 10$. As shown in Figure 3, by an increase in N, the SE value increases with the detectors in question, and this increase can be improved effectively by increasing the number of PU antennas. However, there are limitations in relative addition due to manufacturing technology and portable user volume. There are several antennas in each PU and SU, so in this article, we have considered the number of PU antennas as M and the number of SU antennas as N. Total number of all users is K. As depicted in Figure 3, in MMSE- SIC uplink estimation method, for $N = 3$ and $M \geq 5$, SE will be a little more than 8 bit/s/Hz and for $N = 1$and $M \geq 5$ SE ≥ 6.4 bit/s/Hz, so will have an improvement of about 20% in SE.

Figure 4 shows the total value of SE that can be obtained as a function of NK, calculated, and plotted for the

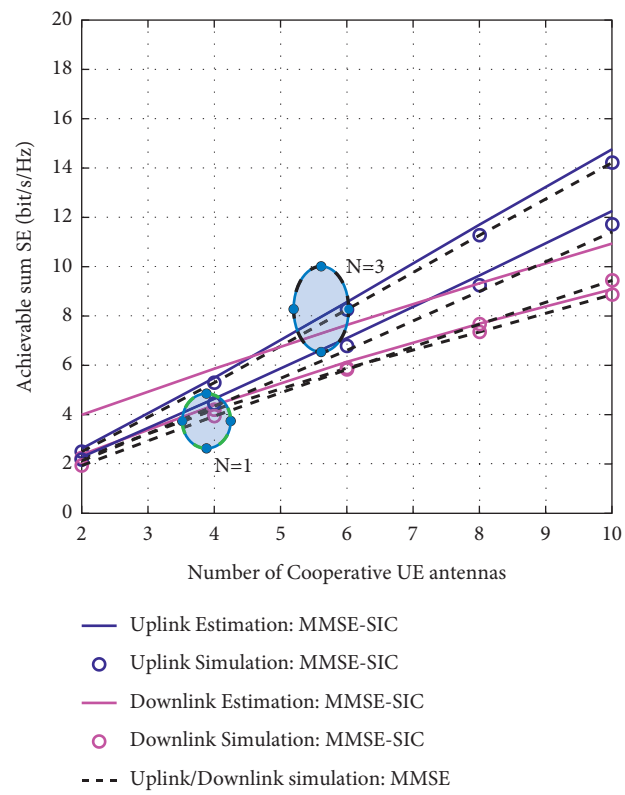

Figure 3: The total amount of obtained SE as a function of the number of PU antennas for. $M = 2, \ldots, 10$ in uplink, downlink for $N = \{1,3\}$, $k = 10$.

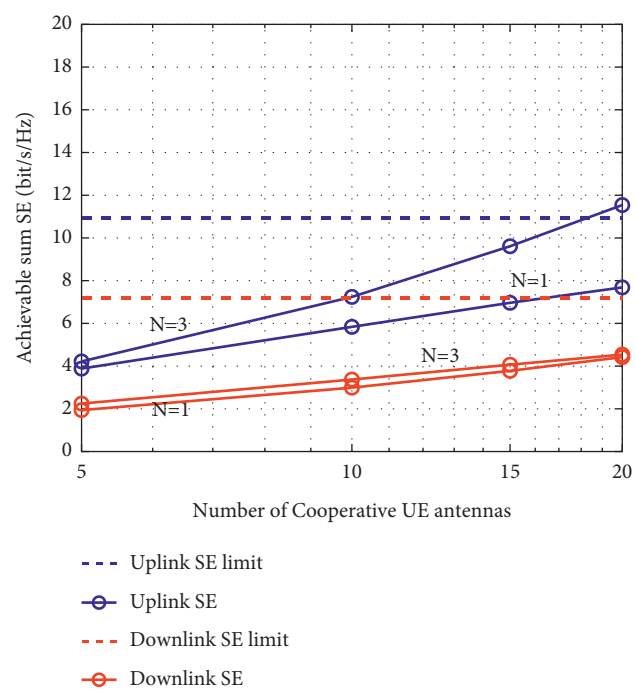

Figure 4: Total SE obtained as a function of $N = \{1,3\}$, $K = 10$ and $\mathbf{M} = 5, \ldots, 20$.

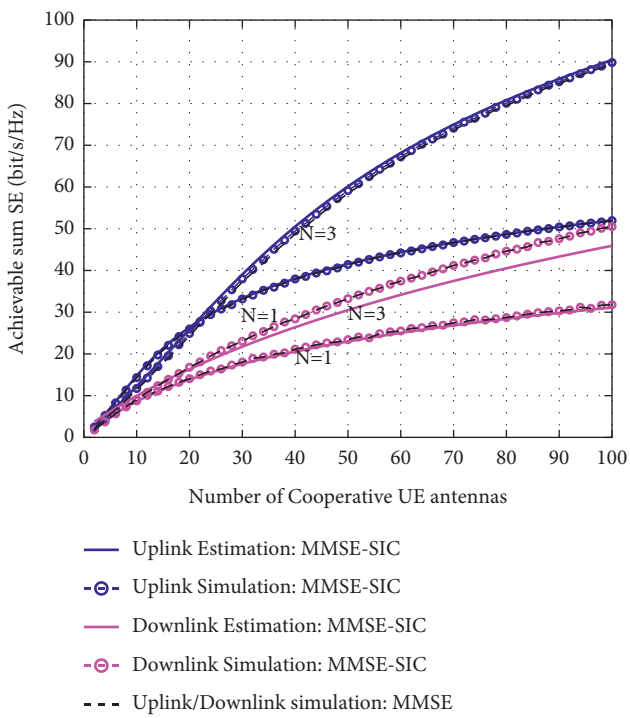

Figure 5: The total amount of obtained SE as a function of the number of PU antennas. $M = 2, \ldots, 100$ in uplink, downlink for $N = \{1,3\}$, $k = 10$.

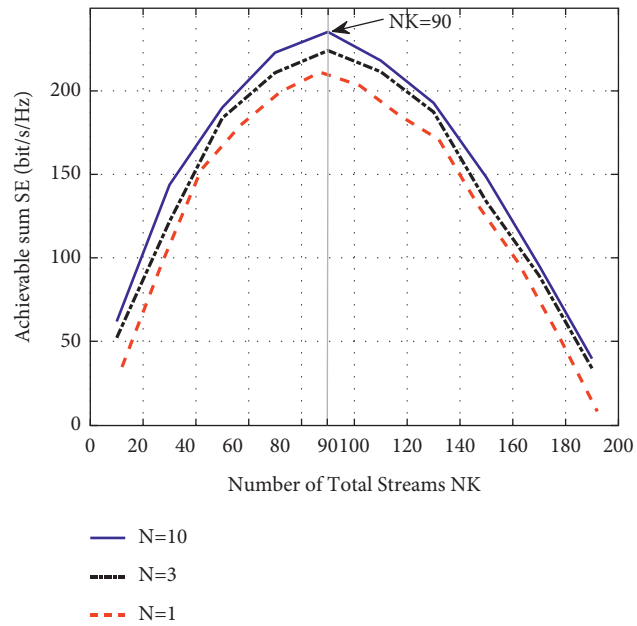

Figure 6: The total amount of SE can be obtained as a function of NK for $N = 1,3,10$ and $\mathbf{M} = 200$.

approximate lower boundary value of the channel capacity for uplink and downlink, respectively. According to Figure 4, as the number of antennas at primary-relay users increases, the amount of SE in the uplink for $N = 3$ approaches the highest possible level of SE. Still, this event occurs around $M = 20$, which is due to the limitations of manufacturing technology of an increasing number of user antenna. On the other hand, for $N = \{1,3\}$, with an increase in the number of users receiving antennas and N, no significant change is obtained near the resulting SE to the absolute limit of SE. The following are two ways to overcome this:

(1) Increasing the number of strings from $N = 3$ to, $N = 5$ for example

(2) Reducing the number of users from $K = 10$ to $K = 5$

With this assumption, cognitive radio (CR) possibility should be considered, and based on beam forming (BF), the maximization of SE in DL should be discussed. Accordingly, modulation effects should be applied in the communication between the primary users to use the SE maximization rate for the subsequent layers by directing the beam in the clusters and using it to the secondary user as the headers of the secondary users.

In Figures 3 and 4, where we considered limitations of manufacturing technology with $M = 10, 20$, it seems we do not have considerable improvement at downlink SE, but when in Figure 5, the number of cooperative user antennas increases to 30 and higher and an appreciable increase will occur in downlink SE in addition to uplink SE improvement to more than 20%. Also, the figure indicates that this incremental relation is not linear.

Figure 6 shows that with the hypothetical increase of NK, that is, the number of exchange strands and K, the amount of SE decreases again from a particular value at the peak of the matter and shows that increasing these two parameters, not only does not increase but tends them to zero; this is a detection method that can effectively increase SE in conventional NK.

The downlink performance is compared in Figure 6 for $N \in \{1, 3, 10\}$. Figure 6 shows that for any given NK, scheduling NK multiantenna users is always beneficial. The optimal NK is around 100, which requires 100 active users per coherence block if $N = 1$. With multiantenna users, more realistic user numbers are sufficient to reach the sweet spot of NK ≈ 100. Therefore, additional user antennas are beneficial to increase the spatial multiplexing in lightly and medium-loaded systems.

6. Conclusion

Separating correlated PU and SU antennas is of vital importance. To this end, we use Kronecker statistical model for channel. We examined and analyzed the extent to which SE can be acquired in a cooperative communication system with each user aware of its own CSI. By estimating CSI in uplink and downlink, we obtained the lower bound value for the total capacity in ergodic form per user by the MMSE-SIC method. We compared these values with the values obtained by the MMSE method. This comparison shows that the MMSE-SIC detection method, such as the linear MMSE method, is highly efficient and can handle users equipped with multiantennas in cooperative communication. In addition, we showed that the SE increases effectively with increasing N. This increase will be to a certain extent. Then decreases again with increasing NK, where this process is independent of the detection method. The results of SE

improvement are presented in uplink and downlink. Calculation results show that additional user antennas are particularly beneficial for SE enhancement when there are few active users in the system. Ten percent of SE improvement and an additional 3–5 data stream numbers are the gain of the proposed detection technique.

Appendix

A. Proof of. $\mathrm{SINR}_{k,i}^{\mathrm{UL}}$

Received signal in the PU relay is $\hat{S}_k$, precoding matrix user $F_k' F_k$, $k = 1, \ldots$ K. Applying linear detector $f_{k,i} = \sqrt{\lambda_{k,i} p_{k,i}} \sum \hat{g}_{k,i}$ to uplink the received signal in PU (A.1) maximizes uplink SE for the $i^{\mathrm{th}} i_{th}$ string for $k^{\mathrm{th}} k_{th}$ user in MMSE detection: $S_k \sim NC(0, I_N)$, $\hat{S}_k$ is estimated transmitted signal [41].

$$Y = \sum_{k=1}^{K} H_k F_k' S_k + n = \sum_{k=1}^{K} G_k \Gamma_k^{(1/2)} P_k^{(1/2)} S_k + n_k, \tag{A.1}$$

$$\begin{aligned} \hat{S}_k &= f_{k,i}^H Y = f_{k,i}^H \left[\sum_{k=1}^{K} H_k F_k' S_k + n \right] \\ &= f_{k,i}^H \left[\sum_{k=1}^{K} G_k \Gamma_k^{(1/2)} P_k^{(1/2)} S_k + n_k \right]. \end{aligned} \tag{A.2}$$

We can estimate noise as $n = Y - \sum_{k=1}^{K} G_k \Gamma_k^{1/2} P_k^{1/2} S_k$; therefore, $f_{k,i}^H n f_{k,i} = f_{k,i}^H [Y - \sum_{k=1}^{K} G_k \Gamma_k^{1/2} P_k^{1/2} S_k] f_{k,i}$, so it can be obtained as $n = f_{k,i}^H [Y - \sum_{k=1}^{K} G_k \Gamma_k^{(1/2)} P_k^{(1/2)} S_k] f_{k,i}$.

Knowing SNR = (P_s/P_n) that P_s and P_n are signal and noise powers, respectively, in calculating the power of noise using its variance, the uncertainty of the channel will be considered.

$$\begin{aligned} P_s &= \left(\Gamma_k^{(1/2)} P_k^{(1/2)}\right)^{(1/2)} \left| f_{k,i}^H \hat{g}_{k,i} \right|^2 = \lambda_{k,i} p_{k,i} \left| f_{k,i}^H \hat{g}_{k,i} \right|^2 \\ P_n &= E\left[nn^H\right] = E\left[\left(f_{k,i}{}^H \left(Y - \sum_{k=1}^{K} G_k \Gamma_k^{(1/2)} P_k^{(1/2)} S_k \right) f_{k,i} \right) \left(f_{k,i}{}^H \left(Y - \sum_{k=1}^{K} G_k \Gamma_k^{(1/2)} P_k^{(1/2)} S_k \right) f_{k,i} \right)^H \right] \\ &= f_{k,i}^H \left[E\left[\mathrm{YY}^H\right] - E\left[\sum_{k=1}^{K} G_k \Gamma_k^{(1/2)} P_k^{(1/2)} G_k \Gamma_k^{(1/2)} P_k^{(1/2)} \right] \right] f_{k,i} \\ &= E\left[f_{k,i}^H \left(\mathrm{YY}^H - \sum_{k=1}^{K} G_k \Gamma_k^{(1/2)} P_k^{(1/2)} \right) f_{k,i} \right], \end{aligned} \tag{A.3}$$

where $\hat{g}_k = \mathrm{vec}(\hat{G}_k)$, $\hat{g}_{k,i}$ is i_{th} column of $\hat{G}_k$.

We have

$$P_n = E\left[\left(f_{k,i}^H \left(\mathrm{YY}^H - \lambda_{k,i} p_{k,i} \hat{g}_{k,i} \hat{g}_{k,i}^H \right) f_{k,i} \right) | \hat{G} \right]. \tag{A.4}$$

Thus, the ultimate SNR in uplink is achieved as follows:

$$\mathrm{SINR}_{k,i}^{\mathrm{UL}} = \frac{\lambda_{k,i} p_{k,i} \left| f_{k,i}^H \hat{g}_{k,i} \right|^2}{\mathbb{E}\left\{ f_{k,i}^H \left(\mathrm{YY}^H - \lambda_{k,i} p_{k,i} \hat{g}_{k,i} \hat{g}_{k,i}^H \right) f_{k,i} | \hat{G} \right\}}. \tag{A.5}$$

Data Availability

The data used in the study are available in the article.

Conflicts of Interest

The authors declare that they have no conflicts of interest.

References

[1] N. Cardona, *Cooperative Radio Communications for Green Smart Environments*, River Publishers Series in Communications, Denmark, 2016.

[2] C.-N. Chuah, J. M. Kahn, D. N. C. Tse, and R. Valenzuela, "Capacity scaling in MIMO wireless systems under correlated fading," *IEEE Transactions on Information Theory*, vol. 48, no. 3, pp. 637–650, 2002a.

[3] D.-S. Shiu, G. J. Foschini, M. Gans, and J. M. Kahn, "Fading correlation and its effect on the capacity of multielement antenna systems," *IEEE Transactions on Communications*, vol. 48, no. 3, pp. 502–513, 2000a.

[4] K. Liu, V. Raghavan, and A. M. Sayeed, "Capacity scaling and spectral efficiency in wideband correlated MIMO channels," *IEEE Transactions on Information Theory*, vol. 49, no. 10, pp. 2504–2526, 2003.

[5] A. S. Y. Poon, R. Brodersen, and D. N. C. Tse, "Degrees of freedom in multiple-antenna channels: a signal space, approach," *IEEE Transactions on Information Theory*, vol. 51, no. 2, pp. 523–536, 2005.

[6] A. M. Sayeed, "2002. Deconstructing multi-antenna fading channels," *IEEE Transactions on Signal Processing*, vol. 50, no. 10, pp. 2563–2579.

[7] V. Veeravalli, Y. Liang, and A. M. Sayeed, "Correlated MIMO wireless channels: capacity, optimal signaling, and asymptotics," *IEEE Transactions on Information Theory*, vol. 51, no. 6, pp. 2058–2072, 2005a.

[8] J. A. Cal-Braz and R. Sampaio-Neto, "Low-complexity sphere decoding detector for generalized spatial modulation systems," *IEEE Communications Letters*, vol. 18, no. 6, pp. 949–952, 2014.

[9] K. Dovelos, M. Matthaiou, H. Q. Ngo, and B. Bellalta, "Massive MIMO with multi-antenna users under jointly correlated ricean fading," in *Proceedings of the ICC 2020-2020 IEEE International Conference on Communications (ICC)*, pp. 1–6, IEEE, Dublin, Ireland, June 2020.

[10] J. Mirzaei, S. ShahbazPanahi, F. Sohrabi, and R. Adve, "Hybrid analog and digital beamforming design for channel estimation in correlated massive MIMO systems," *IEEE Transactions on Signal Processing*, vol. 69, pp. 5784–5800, 2021.

[11] W. Liu, N. Wang, M. Jin, and H. Xu, "Denoising detection for the generalized spatial modulation system using sparse property," *IEEE Communications Letters*, vol. 18, no. 1, pp. 22–25, 2014.

[12] C. Wang, P. Cheng, Z. Chen, J. A. Zhang, Y. Xiao, and L. Gui, "Near- ML low-complexity detection for generalized spatial modulation," *IEEE Communications Letters*, vol. 20, no. 3, pp. 618–621, 2016.

[13] L. Xiao, P. Yang, Y. Xiao et al., "Efficient compressive sensing detectors for generalized spatial modulation systems," *IEEE Transactions on Vehicular Technology*, vol. 66, no. 2, pp. 1284–1298, 2017.

[14] C. M. Yu, S. H. Hsieh, H. W. Liang et al., "Compressed sensing detector design for space shift keying in MIMO systems," *IEEE Communications Letters*, vol. 16, no. 10, pp. 1556–1559, 2012.

[15] C. E. Chen, C. H. Li, and Y. H. Huang, "An improved ordered-block MMSE detector for generalized spatial modulation," *IEEE Communications Letters*, vol. 19, no. 5, pp. 707–710, 2015.

[16] Y. Xiao, Z. Yang, L. Dan, P. Yang, L. Yin, and W. Xiang, "Low complexity signal detection for generalized spatial modulation," *IEEE Communications Letters*, vol. 18, no. 3, pp. 403–406, 2014.

[17] T. Lakshmi Narasimhan and A. Chockalingam, "On the capacity and performance of generalized spatial modulation," *IEEE Communications Letters*, vol. 20, no. 2, pp. 252–255, 2016.

[18] L. He, J. Wang, W. Ding, and J. Song, "Sparse Bayesian learning based symbol detection for generalised spatial modulation in large-scale MIMO systems," in *Proceedings of the IEEE GLOBECOM*, pp. 1–6, San Diego, CA, USA, December 2015.

[19] C. T. Lin, W. R. Wu, and C. Y. Liu, "Low-complexity ML detectors for generalized spatial modulation systems," *IEEE Transactions on Communications*, vol. 63, no. 11, pp. 4214–4230, 2015.

[20] A. Younis, M. D. Renzo, R. Mesleh, and H. Haas, "Sphere decoding for spatial modulation," in *Proceedings of the IEEE Int. Conf. Commun. (ICC),*, pp. 1–6, Kyoto, Japan, June 2011.

[21] A. Younis, S. Sinanovic, M. Di Renzo, R. Mesleh, and H. Haas, "Generalised sphere decoding for spatial modulation," *IEEE Transactions on Communications*, vol. 61, no. 7, pp. 2805–2815, 2013.

[22] A. Dytso, R. Bustin, D. Tuninetti, N. Devroye, H. V. Poor, and S. Shamai Shitz, "On communication through a Gaussian channel with an MMSE disturbance constraint," *IEEE Transactions on Information Theory*, vol. 64, no. 1, pp. 513–530, 2018.

[23] S. Imam, M. Zaher, and A. El-Mahdy, "Block diagonalization based interference cancellation in uplink multi user cooperative communication system," in *Proceedings of the IEEE 10th Annual Information Technology, Electronics and Mobile Communication Conference (IEMCON)*, Vancouver, BC, Canada, October 2019.

[24] T. C. Mai, H. Q. Ngo, and T. Q. Duong, "Downlink spectral efficiency of cell-free massive MIMO systems with multi-antenna users," *IEEE Transactions on Communications*, vol. 68, no. 8, pp. 4803–4815, 2020.

[25] M. Trik, S. Pour Mozaffari, and A. M. Bidgoli, "Providing an Adaptive Routing along with a Hybrid Selection Strategy to Increase Efficiency in NoC-Based Neuromorphic Systems," *Computational Intelligence and Neuroscience*, vol. 2021, Article ID 8338903, 8 pages, 2021.

[26] M. G. Berceanu, C. Voicu, and S. Halunga, "The performance of an uplink Large Scale MIMO system with MMSE-SIC detector," in *Proceedings of the 2019 International Conference on Military Communications and Information Systems (ICMCIS)*, pp. 1–4, IEEE, Budva, Montenegro, May 2019.

[27] V. Tuzlukov, "Interference cancellation for MIMO systems employing the generalized receiver with high spectral efficiency," *WSEAS Transactions on Signal Processing*, vol. 17, pp. 1–15, 2021.

[28] X. Cheng, C. X. Wang, D. I. Laurenson, S. Salous, and A. V. Vasilakos, "An adaptive geometry-based stochastic model for non-isotropic MIMO mobile-to-mobile channels," *IEEE Transactions on Wireless Communications*, vol. 8, no. 9, pp. 4824–4835, 2009.

[29] O. Simeone and U. Spagnolini, "Lower bound on training-based channel estimation error for frequency-selective block-fading Rayleigh MIMO channels," *IEEE Transactions on Signal Processing*, vol. 52, no. 11, pp. 3265–3277, 2004.

[30] J. P. Kermoal, L. Schumacher, K. I. Pedersen, P. E. Mogensen, and F. Frederiksen, "A stochastic MIMO radio channel model with experimental validation," *IEEE Journal on Selected Areas in Communications*, vol. 20, no. 6, pp. 1211–1226, 2002a.

[31] X. Li, E. Bjornson, S. Zhou, and J. Wang, "Massive MIMO with multi-antenna users: when are additional user antennas beneficial?" in *Proceedings of the 2016 23rd International Conference on Telecommunications (ICT)*, Thessaloniki, Greece, May 2016.

[32] C. L. Anioke, C. Nnamani, and C. I. Ani, "Review of wireless MIMO channel models," *Nigerian Journal of Technology*, vol. 35, no. 2, p. 381, 2016.

[33] V. Raghavan, J. H. Kotecha, and A. M. Sayeed, "Why does the kronecker model result in misleading capacity estimates?" *IEEE Transactions on Information Theory*, vol. 56, no. 10, pp. 4843–4864, 2010.

[34] E. Bjornson and B. Ottersten, "A framework for training-based estimation in arbitrarily correlated rician MIMO channels with rician disturbance," *IEEE Transactions on Signal Processing*, vol. 58, no. 3, pp. 1807–1820, 2010.

[35] H. Q. Ngo, E. G. Larsson, and T. L. Marzetta, "Energy and spectral efficiency of very large multiuser MIMO systems," *IEEE Transactions on Communications*, vol. 61, no. 4, pp. 1436–1449, 2013.

[36] T. Yoo and A. Goldsmith, "Capacity and power allocation for fading MIMO channels with channel estimation error," *IEEE Transactions on Information Theory*, vol. 52, no. 5, pp. 2203–2214, 2006.

[37] J. Hoydis, S. ten Brink, and M. Debbah, "Massive MIMO in the UL/DL of cellular networks: how many antennas do we need?" *IEEE Journal on Selected Areas in Communications*, vol. 31, no. 2, pp. 160–171, 2013.

[38] X. Li, E. Bjornson, E. G. Larsson, S. Zhou, and J. Wang, "A multi cell MMSE detector for massive MIMO systems and new large system analysis," *Proceedings of the IEEE GLOBECOM*, , San Diego, CA, USA, December 2015.

[39] P. Bagot, M. Beach, A. Nix, J. McGeehan, and P. Moss, "Adaptive Broadcast Techniques for Digital Terrestrial Television," Technical Report TD-09-041, Ferrara, Italy, 2014.

[40] B. Nosrat-Makouei, J. G. Andrews, and R. W. Heath, "MIMO interference alignment over correlated channels with imperfect CSI," *IEEE Transactions on Signal Processing*, vol. 59, no. 6, pp. 2783–2794, 2011.

[41] S. Park, A. Q. Truong, and T. H. Nguyen, "Power control for sum spectral efficiency optimization in MIMO-NOMA systems with linear beamforming," *IEEE Access*, vol. 7, Article ID 10605, 2019.

Hindawi
International Journal of Antennas and Propagation
Volume 2022, Article ID 3505181, 11 pages
https://doi.org/10.1155/2022/3505181

Research Article

Analysis of Joint Angular Distribution for Nonreciprocal Beams via the Mixture of Gaussian Distribution Based on Ray-Tracing

Jiachi Zhang,[1,2] Liu Liu,[1] Zhenhui Tan,[1] Kai Wang,[1] and Tao Zhou[1]

[1]*School of Electronic and Information Engineering, Beijing Jiaotong University, Beijing 100044, China*
[2]*School of Rail Transportation, Shandong Jiaotong University, Jinan 250357, China*

Correspondence should be addressed to Liu Liu; liuliu@bjtu.edu.cn

Received 29 December 2021; Revised 20 March 2022; Accepted 12 April 2022; Published 9 May 2022

Academic Editor: Angelo Liseno

Multiple-input and multiple-output (MIMO) technology can not only provide huge data rates but also overcome the severe propagation attenuation effect, especially in millimeter-wave (mmWave) bands by utilizing beamforming. The nonreciprocal beam is a novel transmission pattern, which indicates that transceivers adopt asymmetrical beamwidths. Such a special pattern can achieve fast beam alignment and alleviate equipment costs. Thorough knowledge of the corresponding wireless channel is pivotal to the system design and optimization, which remains to be investigated. In this paper, we first propose a 3-dimensional (3-D) channel model based on ray-tracing, which is capable of reflection simulation. Based on this model, the ray-based beamforming mechanism is illustrated. The angular distribution is pivotal to beam channel modeling and characterization since transceiver beams filter rays in the angular domain. Then, we conduct an omnidirectional antenna-based channel simulation in an urban macro-cell scenario via the ray-tracing platform. On this basis, we focus on the distribution of the quasiangles, i.e., angles between departure/arrival reflected rays and the line-of-sight (LoS) path. We find that gamma distribution is a better option to fit the quasiarrival angular distribution than the von Mises distribution. Furthermore, to characterize the relationship between quasiangles of departure (AoD) and quasiangles of arrival (AoA), the Gaussian mixture model (GMM) is adopted and the expectation-maximization (EM) algorithm is used to estimate the unknown parameters of GMM. Our findings provide useful insights to beam channel modeling, which should take the joint angular distribution into consideration.

1. Introduction

With the burst use of video streaming, immersive VR/AR, and the Internet-of-Things (IoT), the proliferation of the fifth-generation (5G) mobile communication system boosts wireless mobile connectivity, enhances data rate, and yields great user satisfaction [1]. Enhanced mobile broadband (eMBB) communication is one of three primary 5G New Radio (NR) use cases defined by the 3GPP, which aims to achieve a high peak user data rate of 1 Gbps. Moreover, this target is set to 1 Tbps in the next sixth-generation (6G) communication system, which brings new challenges and receives extensive attention both from academia and industry. Under such a circumstance, the trend of exponentially growing demand in mobile data drives wireless networks to migrate to higher frequency bands.

Millimeter-wave (mmWave), spanning the spectrum from 30 GHz to 300 GHz, is envisioned as the key technology of the next-generation mobile communication system, including both beyond 5G (B5G) and 6G communication systems [2]. However, the mmWave band leads to unbearable propagation loss due to a variety of factors including atmospheric absorption, basic Friis transmission-effect, and low penetration. To address this issue, it is widely believed that mmWave propagation together with the multiple-input and multiple-output (MIMO)-based beamforming technology can handle the drastic increase of mobile data traffic [3].

Beamforming employs facilities to vary the beams' power and their directions with the aid of amplitude/phase

variations. Modern wireless system uses antenna arrays instead of a single antenna to synthesize a beam. Ideally, transceivers' beams point to each other all the time, i.e., beam alignment can provide a high propagation gain. However, perfect beam alignment incurs high delay overhead, especially over fast fading channel scenarios like high-speed railways (HSR), vehicle-to-vehicle/infrastructure (V2V/I) communications, and unmanned aerial vehicles (UAV). Conventional beam pattern adopts the symmetric beamwidth, reciprocal beams in brief, which makes finding a perfect match pair of beams time-consuming by exhaustive search method. Furthermore, the computational complexity explodes when using narrow-width beams. Besides, such a beam pattern requires the same channels of both transmitter (Tx) and receiver (Rx), which incurs substantial hardware complexity and expensive hardware costs. To cope with these issues, some prevailing technologies, such as hybrid beamforming (the combined analog and digital beamforming), low-resolution analog-to-digital converters (ADCs), and digital-to-analog converter (DACs) technologies, have been thoroughly investigated. Nevertheless, the former requires a heavy beam training overhead for channel estimation, whereas the latter uses complex iterative algorithms to recover the lost information at the receiver.

The authors in [4, 5] first proposed a concept of the full-digital arrays with nonreciprocal transmitting and receiving beam patterns. The novelty of this strategy lies in the fact that the nonreciprocal beam patterns use an unequal number of Tx and Rx channels, or beams with different widths, which makes the transmitting and receiving patterns asymmetrical. Figure 1 presents a diagram of this pattern. As seen in this figure, the base station (BS) uses a narrow-width beam to transmit signals in the downlink, whereas the mobile station (MS) adopts a wide-width beam to receive. In the uplink, the usage of beams is quite opposite. Benefiting from this flexible architecture, this pattern owns merits like wide beam scanning range and low hardware complexity. Therefore, it can achieve higher energy and cost efficiencies. This nonreciprocal pattern could not only release the burden of data processing as well as reduce the hardware cost and power consumption of the entire system but also can realize efficient beam alignment quickly. However, such a pattern leads to the nonreciprocity for uplink and downlink channels, indicating that time division duplex (TDD)-based systems cannot implement this strategy directly.

A thorough understanding of the wireless channel is a prerequisite for further system design, algorithm optimization, and network deployment. Generally, current prevailing channel models mainly contain the geometry-based stochastic models (GBSMs) and the ray-tracing at the mmWave bands. The former model is widely used due to its mathematical tractability, especially for the regular-shaped GBSM (RS-GBSM) [6]. Ray-tracing is validated by extensive comparisons with actual measured data [7]. Based on this, a huge volume of MIMO-related ray-tracing works are also performed. Nonetheless, some of them use the horn antenna to mimic the beamforming [8], whereas others consider the MIMO array response but fail to investigate the beam filtering effect [9]. As for the beam channel measurement works, most of them are

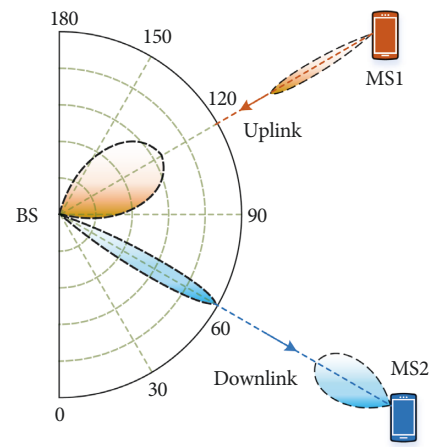

Figure 1: Diagram of the nonreciprocal beam patterns.

performed on symmetrical beam patterns, like [10, 11]. To our best knowledge, few related works on the asymmetrical pattern have been studied until now, which remains a gap to be investigated thoroughly and we will address it herein.

To this end, we aim to propose a beam channel model based on the ray-tracing and investigate the stochastic channel properties of high reflection bounces. The motivations and our contributions are presented as follows:

(1) We propose a 3-dimensional (3-D) MIMO channel model based on the ray-tracing, which incorporates the multiple-bounce reflection propagations. Our proposed model is elaborated from the phase expression of propagation distance and Doppler shift. Then, we prove the feasibility of beamforming and enable our model capable of beamforming with different beamwidths and steering directions.

(2) To get the full knowledge of channel angular information of multiple-bounced paths, we analyze the angular distribution relationship based on a ray-tracing platform in an urban street scenario. Specifically, we focus on transceiver angular distributions on the assumption of perfect beam alignment, i.e., the angles between Tx/Rx and departure/arrival rays, denoted as quasi-angles of arrival (AoAs)/departure (AoDs) in brief.

(3) We focus on the arrival side and find that the gamma distribution is a better option than the von Mises distribution to characterize the distribution of quasi-AoAs of multiple reflection bounces. Moreover, to obtain the angular distribution at the departure side, we employ the Gaussian mixture model (GMM) to depict the relationship between quasi-AoAs and quasi-AoDs. Besides, transceiver beams are considered as two constraints of the GMM.

The remainder of this paper proceeds as follows. In Section 2, we present an overview of the mmWave beam channel modeling. Section 3 introduces the proposed channel model in detail. In Section 4, we analyze the angular distribution based on a ray-tracing platform, and the final relevant conclusions are drawn in Section 5.

Table 1: Related mmWave channel measurements.

Ref.	Scenario	Freq. (GHz)	BW (MHz)	Method	MIMO array
[12]	ID	28	500	HA	VA
[13]	ID	28/38	4000	HA	VA
[14]	Office	28/73	400	HA	1×1
[15]	OD	28/38	400/750	HA	1×1
[16]	ID	28	125	PA	4×4
[17]	ID and OD	28/32/39	1000	PA	4×4
[18]	ID	60	1000	PA	8×32

ID: indoors; OD: outdoors; BW: bandwidth; HA: horn antenna; PA: phased-array; VA: virtual array.

Table 2: Important parameter definitions.

Parameter	Definition
T_p, R_q, r_n	The p-th Tx, q-th Rx, n-th ray
$D_n(t)$	Path distances of the n-th ray
$\alpha_n^H(t), \alpha_n^V(t)$	Azimuth/elevation AODs of r_n
$\alpha_{\mathrm{bm}}^H(t), \alpha_{\mathrm{bm}}^V(t)$	Azimuth/elevation angles of Tx beam-steering direction
$\beta_{\mathrm{bm}}^H(t), \beta_{\mathrm{bm}}^V(t)$	Azimuth/elevation angles of Rx beam-steering direction
$\beta_n^H(t), \beta_n^V(t)$	Azimuth/elevation AOAs of r_n
$\tilde{\alpha}_n(t), \tilde{\beta}_n(t)$	Quasi-AOD/AOA of r_n
$\vartheta_{n,m}$	The m-th LCS incident angle of r_n
δ_T, δ_R	Adjacent element spacing of Tx/Rx
α_W, β_W	Beamwidths of Tx/Rx
$\gamma_{\mathrm{MS}}^H(t), \gamma_{\mathrm{MS}}^V(t)$	Azimuth/elevation angles of MS velocity

2. Literature Review

In terms of mmWave beam channel measurement, numerous works have been performed with respect to different frequency carriers. These works can be generally classified into two types based on beam synthesis method, i.e., horn-based measurement and phased-array-based measurement. The first method emulates a beam with a certain beam width by using a horn antenna, which is widely used due to its simple implementation. Related works are like [12–15]. Indeed, this method can work to a large extent by designing an antenna pattern similar to an array response. However, the beam alignment needs to be achieved via the real-time adjustment of antenna rotation.

Other works were conducted based on the phased-array antennas, which form real beams in the desired direction with appropriate power. A list of related mmWave channel measurement campaigns is presented in Table 1. However, due to the high equipment cost and expenditure, few works have been performed, not to mention the complete channel characterization of different beamwidths. Hence, there is a great demand for an accurate theoretical model with the ability of beamforming simulation.

The measurement-based channel modeling indeed provides some insightful mmWave beam models, but it cannot cover a wide range of beamwidth, whereas theoretical models can fill this research gap. Currently, the theoretical methods of mmWave channel modeling can be classified into two types, i.e., the deterministic and stochastic methods. As for the former one, ray-tracing is widely used due to its high accuracy, especially considering that electronic wave exhibits an evident mechanism of reflection at high-frequency bands. Some works have combined ray-tracing with beamforming, like [19]. Moreover, some commercial simulation platforms, e.g., Wireless Insite, has already incorporated beamforming into ray-tracing [20]. However, RT is time-consuming when considering multiple bounces and cannot efficiently emulate the scattering mechanism.

In terms of the stochastic method, a prevailing scheme is the geometry-based stochastic method (GBSM) [21], which is widely adopted in some 5G organization standards, e.g., COST2100 and COST IC1004 channel models, QuaDRiGa, etc. [22]. Much work has been performed on the GBSM, representative works like [23–25]. Moreover, the application of GBSM involves rich scenarios, like V2V and UAV [26, 27]. Conventional GBSM assumes that channel parameters follow a certain stochastic process, which imposes little computational burdens and can be quickly adapted to various scenarios by changing parameter values. Other works aim to apply beamforming into GBSM, like [28]. However, the AoD distributions of these works are obtained via geometric manipulations based on the single-bounced or double-bounced assumption, which faces exceptional geometric difficulties for higher bounces.

Another stochastic method is the propagation-graph (PG) theory, which abstracts the propagation environment into a directed graph [29]. This method requires much less computational complexity compared to RT. It can yield a satisfying simulation accuracy since that it mainly considers the scattering mechanism, enriching the "tails" of multipath taps in channel impulse response (CIR). Moreover, some works applied scattering and diffraction models into PG to enhance modeling accuracy [29, 30]. Nevertheless, these works all fail to incorporate the beamforming effect while simulating the multiple-input and multiple-output (MIMO) system.

As for works on the nonreciprocal beam patterns, current efforts are mainly devoted to antenna design and implementation. A concept of a full-duplex nonreciprocal-beam-steering model is proposed based on the metasurface in [31], which uses nonreciprocal radiation beams to realize point-to-point telecommunications. Furthermore, the authors in [32] proposed a nonreciprocal-beam phased-array based on the transistor-based nonreciprocal phase shifters, which can exhibit different beams for transmission and reception states. Notably, the above works are performed on the metasurface, which is beyond the scope of commercial mobile communications. Since being investigated in [4], nonreciprocal beam patterns attract much attention due to the low hardware complexity of radio frequency (RF) chains. In [33], the authors designed an asymmetrical transceiver architecture for massive MIMO systems, which consists of a different number of RF chains for Tx and Rx. Reference [34] reports a high-performance wideband frequency synthesizer for nonreciprocal beams. However, to our best knowledge, little research on channel modeling and characterization over nonreciprocal beam patterns has been performed until now.

3. System Model

3.1. Ray-Tracing-Based Channel Model. For further derivations and descriptions, we list some important variables together with definitions in Table 2. The channel transfer function (CTF) obtained by ray-tracing is the sum of all possible reflected paths and line-of-sight (LoS) path. Different from the conventional expression, we take the channel gain as well as the phase information into account. Without loss of generality, we use the word "ray" instead of path in the following text since that our proposal is inspired by ray-tracing. Specifically, the CTF of the n-th ray from the the p-th Tx (T_p) to the q-th Rx (R_q) can be formulated as

$$h_{pq,n}(t,\tau) = \begin{bmatrix} F_{R,q,V}(\alpha_n^H, \alpha_n^V) \\ F_{R,q,H}(\alpha_n^H, \alpha_n^V) \end{bmatrix}^T \begin{bmatrix} \sqrt{\kappa_n^{-1}}\, e^{j\Theta_n^{VV}} & e^{j\Theta_n^{VH}} \\ e^{j\Theta_n^{HV}} & \sqrt{\kappa_n^{-1}}\, e^{j\Theta_n^{HH}} \end{bmatrix} \begin{bmatrix} F_{T,p,V}(\beta_n^H, \beta_n^V) \\ F_{T,p,H}(\beta_n^H, \beta_n^V) \end{bmatrix} g_n \cdot e^{j2\pi D_n/\lambda} \cdot e^{j2\pi \nu_n t} \cdot e^{j\eta_n} \cdot \omega_p \underbrace{e^{j2\pi \vec{r}_p \cdot \left(\vec{\Phi}_n^D - \vec{\Phi}_{bm}^D\right)/\lambda}}_{A1} \cdot \omega_q \underbrace{e^{j2\pi \vec{r}_q \cdot \left(\vec{\Phi}_n^A - \vec{\Phi}_{bm}^A\right)/\lambda}}_{A2} \cdot \delta\left(\tau - \tau_{p,q,n}(t)\right), \tag{1}$$

where $F_{R,q,V}$ and $F_{R,q,H}$ are the radiation patterns of the q-th receiver antenna element for vertical and horizontal polarizations, respectively. $F_{T,p,V}$ and $F_{T,p,H}$ denote the radiation patterns of the p-th transmit antenna element for vertical and horizontal polarizations, respectively. Parameters $\Theta_n^{VV}, \Theta_n^{VH}, \Theta_n^{HV}$, and Θ_n^{HH} refer to the initial phases of the n-th ray for 4 different polarization combinations, i.e., vertical-vertical (VV), vertical-horizontal (VH), horizontal-vertical (HV), and horizontal-horizontal (HH). κ_n is the corresponding cross polarization power ratio between H and V, and λ is the wavelength. D_n means the propagation distance from Tx center to Rx center. $D_{pq,n}$ is the propagation distance of the n-th reflected path from T_p to R_q, and $\tau_{p,q,n}$ is the corresponding propagation delay. g_n is the path gain after M reflection bounces, which can be expressed as

$$g_n = \prod_{m=1}^{M} \Gamma_m\left(\vartheta_{n,m}\right) \cdot \frac{\lambda}{4\pi D_{pq,n}}, \tag{2}$$

where ϑ_m is the incident angle of the m-th reflection and Γ_m is the corresponding Fresnel reflection coefficient concerning ϑ_m.

In equation (1), η_n is the additional phase caused by reflection interaction and initial phase. $\vec{\Phi}_n^D$ is the departure angle unit vector of the n-th ray with the elevation angle of departure (EAOD) β_n^V and the azimuth angle of departure (AAOD) β_n^H. $\vec{\Phi}_{\mathrm{bm}}^D$ is the beam-steering angle unit vector of Tx, which consists of EAOD β_{bm}^V and AAOD β_{bm}^H. The detailed expression of $\vec{\Phi}_n^D$ is

$$\vec{\Phi}_n^D = \begin{bmatrix} \cos\beta_n^H \cdot \cos\beta_n^V \\ \cos\beta_n^H \cdot \sin\beta_n^V \\ \sin\beta_n^H \end{bmatrix}^T. \tag{3}$$

Similarly, the arrival angle unit vector $\vec{\Phi}_n^A$ of the n-th ray with the elevation angle of arrival (EAOA) α_n^V and the azimuth angle of arrival (AAOA) α_n^H can be marked as

$$\vec{\Phi}_n^A = \begin{bmatrix} \cos\alpha_n^H \cdot \cos\alpha_n^V \\ \cos\alpha_n^H \cdot \sin\alpha_n^V \\ \sin\alpha_n^H \end{bmatrix}^T. \tag{4}$$

Parameters $\vec{r}_p = (x_p', y_p', z_p')$ and $\vec{r}_q = (x_q'', y_q'', z_q'')$ denote the corresponding coordinates of T_p and R_q in the local coordinate systems (LCS), i.e., $O'(x', y', z')$ and $O''(x'', y'', z'')$, respectively. ν_n is the Doppler shift caused by the movement of mobile station (MS), which is calculated as

$$\nu_n = \vec{\nu}_{MS} \cdot \vec{\Phi}_n^A, \tag{5}$$

where

$$\vec{\nu}_{\mathrm{MS}} = \nu_{\mathrm{MS}} \begin{bmatrix} \cos\gamma_{\mathrm{MS}}^H \cdot \cos\gamma_{\mathrm{MS}}^V \\ \cos\gamma_{\mathrm{MS}}^H \cdot \sin\gamma_{\mathrm{MS}}^V \\ \sin\gamma_{\mathrm{MS}}^H \end{bmatrix}^T, \tag{6}$$

where variable ν_{MS} means the MS speed.

3.2. MIMO-Based Beamforming Effects. MIMO-based beamforming technology can overcome the severe propagation attenuation for mmWave communications. In this subsection, we aim to illustrate the mechanism of MIMO-enabled beamforming. We use the phased array to synthesize the digital beams, which means that each antenna element is assigned with a RF converter. Besides, each channel is assigned with a weight and additional phase to synthesize a desirable beamwidth and beam-steering direction. On the assumption of far-field condition, we adopt the 2-dimensional uniform rectangular array (URA) and the phase parts $A1$ in equation (1) can be characterized by the Tx array steering vector, i.e.,

$$\begin{aligned} \mathbf{p}\left(\alpha^H, \alpha^V\right) &= \left[e^{jk_x x_m + k_y y_{m'}}\right]^T, \\ k_x &= k\sin\alpha^V \cos\alpha^H, \\ k_y &= k\sin\alpha^V \sin\alpha^H, \\ x_m &= \left(m - 0.5(M+1)\delta_T\right), \\ y_{m'} &= \left(m' - 0.5(M+1)\delta_T\right), \end{aligned} \tag{7}$$

where $m = 1, \ldots, N_t^H, m' = 1, \ldots, N_t^V$. We assume that the origin of the LCS is located at the array center. $k = 2\pi/\lambda$ is

the wave number. N_t^H, N_t^V mean the Tx and Rx antenna element number along the horizontal and vertical directions, respectively. Furthermore, each element channel is assigned with a weight to formulate an idea beam shape. Consequently, the synthesis of digital beamforming can be regarded as the design of a finite impulse response (FIR) filter. Herein, we adopt the Dolph-Chebyshev window function $\omega_d = [\omega_n]_{N\times 1}$, which can achieve the lowest sidelobe level (SLL) for a given beamwidth among all weight-based beam designing methods [35]. It can be expressed as equation (8), where $N \in \{N_t^H, N_r^H\}$.

$$\omega_n = \begin{cases} \dfrac{z^{N-1}}{2}, n = 1, \\ \displaystyle\sum_{i=1}^{n-1} \frac{0.5(N-1)(n-2)!(N-i-1)!}{(n-i)!(i-1)!(N-i-1)!(N-n)!} z^{N-2n+1}\left(z^2-1\right)^{n-i}, \dfrac{2 \le n \le N}{2+1}, \omega_{N+1-n}, \dfrac{n \ge N}{2+1}. \end{cases} \tag{8}$$

In equation (8), function $(\cdot)!$ means the factorial function, and z is an auxiliary variable with an expression of

$$z = \begin{cases} \dfrac{\cos\left[0.5\pi(N-1)^{-1}\right]}{\cos\left[\pi\, d\lambda^{-1}\sin\alpha_W\right]}, \alpha_W \text{isconst}, \\ \cosh\left[\dfrac{\operatorname{arcosh}\left(\sqrt{10^{-\mathrm{SLL}/10}}\right)}{N-1}\right], \mathrm{SLL}\text{isconst}. \end{cases} \tag{9}$$

The first case of z means that the main lobe width α_W is a constant while designing, whereas the second case refers that the SLL is determined in decibel scale regardless the main lobe width. As for the desired beam-steering direction $\Omega_s^D = (\alpha_s^H, \alpha_s^V)$, ω_d should be modified by $\mathbf{p}(\alpha_s^H)$ and $\mathbf{p}(\alpha_s^V)$, and the final corresponding expression of the beam response $B(\alpha) = B(\alpha^H)B(\alpha^V)$, and

$$B\left(\alpha^i\right) = \left(\boldsymbol{\omega}_d^i \odot \mathbf{p}\left(\alpha_s^i\right)\right)^T \mathbf{p}\left(\alpha^i\right), \tag{10}$$

where $i \in \{H, V\}$, and symbol $\odot$ means the element-wise operator. The major merits of the Dolph-Chebyshev window function consist of two aspects. Importantly, it can achieve the minimum average SLL while guaranteeing a constant main lobe width. Meanwhile, it can provide the narrowest beamwidth while guaranteeing a constant SLL. As such, we can roughly regard the filter gain as 1 within the passband frequency range and 0 for the stopband case, i.e.,

$$B\left(\Omega^D\right) \approx \begin{cases} 1, \Omega^D \in \left[\alpha_s^H - 0.5\alpha_W^H, \alpha_s^H + 0.5\alpha_W^H\right] \times \left[\alpha_s^V - 0.5\alpha_W^V, \alpha_s^V + 0.5\alpha_W^V\right], \\ 0, \Omega^D \notin \left[\alpha_s^H - 0.5\alpha_W^H, \alpha_s^H + 0.5\alpha_W^H\right] \times \left[\alpha_s^V - 0.5\alpha_W^V, \alpha_s^V + 0.5\alpha_W^V\right]. \end{cases} \tag{11}$$

Finally, the final beam-enabled CTF is expressed as

$$h_n\left(t, \tau, \Omega_n^D, \Omega_n^A\right) = h_n\left(t, \tau, \Omega_n^D, \Omega_n^A\right) \cdot B\left(\Omega^D\right) \cdot B\left(\Omega^A\right), \tag{12}$$

where $\Omega_n^D = \{\alpha_n^H, \alpha_n^V\}, \Omega_n^A = \left\{\beta_n^H, \beta_n^V\right\}$, and

$$h_n\left(t, \tau, \Omega_n^D, \Omega_n^A\right) = \begin{bmatrix} F_{R,q,V}\left(\alpha_n^H, \alpha_n^V\right) \\ F_{R,q,H}\left(\alpha_n^H, \alpha_n^V\right) \end{bmatrix}^T \begin{bmatrix} \sqrt{\kappa_n^{-1}}\, e^{j\Theta_n^{VV}} & e^{j\Theta_n^{VH}} \\ e^{j\Theta_n^{HV}} & \sqrt{\kappa_n^{-1}}\, e^{j\Theta_n^{HH}} \end{bmatrix} \begin{bmatrix} F_{T,p,V}\left(\beta_n^H, \beta_n^V\right) \\ F_{T,p,H}\left(\beta_n^H, \beta_n^V\right) \end{bmatrix} g_n \cdot e^{j2\pi D_n/\lambda} \cdot e^{j2\pi\nu_n t} \cdot e^{j\eta_n} \delta(\tau - \tau_n). \tag{13}$$

It can be seen that the combined effect of all transceivers' elements is equivalent to the Dolph-Chebyshev filter. Therefore, the antenna element index is omitted in this formula.

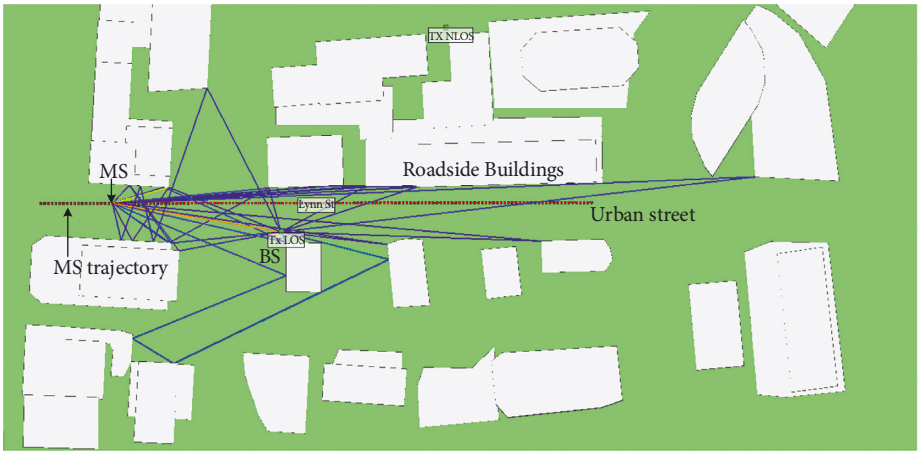

Figure 2: A bird view of the macro-cell urban street scenario.

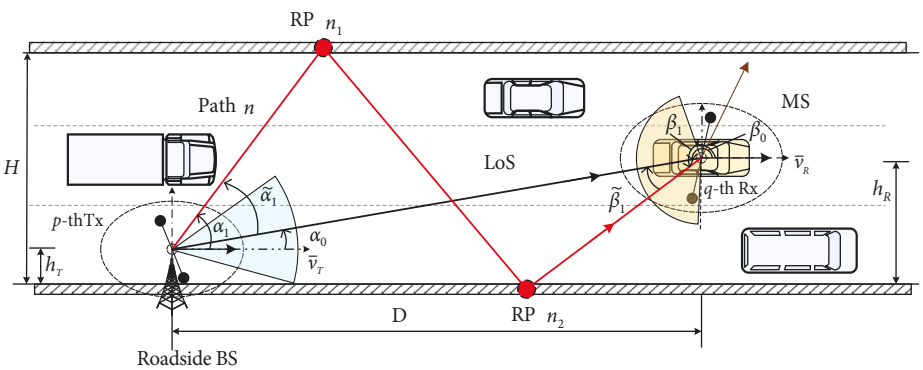

Figure 3: A diagram of the proposed quasiangles.

Table 3: Parameter settings.

Parameter	Value
Frequency carrier	28 GHz
BS position	(20, 0, 25) m
Initial MS position ($t = 0s$)	(−10, 10, 1.5) m
MS velocity vector	(0, 16.67, 0) m/s
Street segment length	147 m
Antenna array	SISO
Antenna pattern	Omnidirectional
Main street size	1 m × 10 m

4. Ray-Tracing-Based Channel Characterization

4.1. Distribution of Quasi-AoAs. The above section elaborates on the proposed MIMO-enabled beamforming channel model based on ray-tracing. In this section, we will investigate the angular properties of the beam channel based on a commercial ray-tracer platform. It is noteworthy that the simulation is performed via this platform without considering the beam effects, i.e., it is conducted based on the omnidirectional antenna. The nonreciprocal beams are considered as two constraints based on the conclusions in equation (11).

The simulation is conducted based on the Wireless Insite, a commercial ray-tracing platform with high simulation efficiency. As shown in Figure 2, the roadside BS communicates with the moving vehicle in an urban street. Furthermore, we simplify this cellular-assisted vehicle communication scenario and present in Figure 3. Note that single-input and single-output (SISO) omnidirectional antenna pattern is used in the simulation and the beam effect is realized for each ray according to equation (11). The BS is located at the roadside with a height of 10 m, whereas the MS with an Rx mounted on the vehicle moves forwards along the main street at a speed of 60 km/h and a 147-meters-long street is simulated. Tall buildings are around the street with heights larger than that of BS. Consequently, scarce reflected rays come from the top obstacles and most of the received rays differ dramatically in the horizontal plane. Detailed values of the simulation parameters are presented in Table 3.

As mentioned earlier, beams act like a spatial filter that poses effects on rays with different angular information. Figure 4 compares the filtered rays via nonreciprocal beams. Red lines indicate reflected rays with higher received power, whereas brown ones represent lower received power, and green lines mean the lowest power. Obviously, this special pattern yields different filtering results on reflected rays. Therefore, to obtain the beam-enabled stochastic channel model, the primary pivotal task is to investigate the angular distribution of AoAs and AoDs. Figure 5 presents the

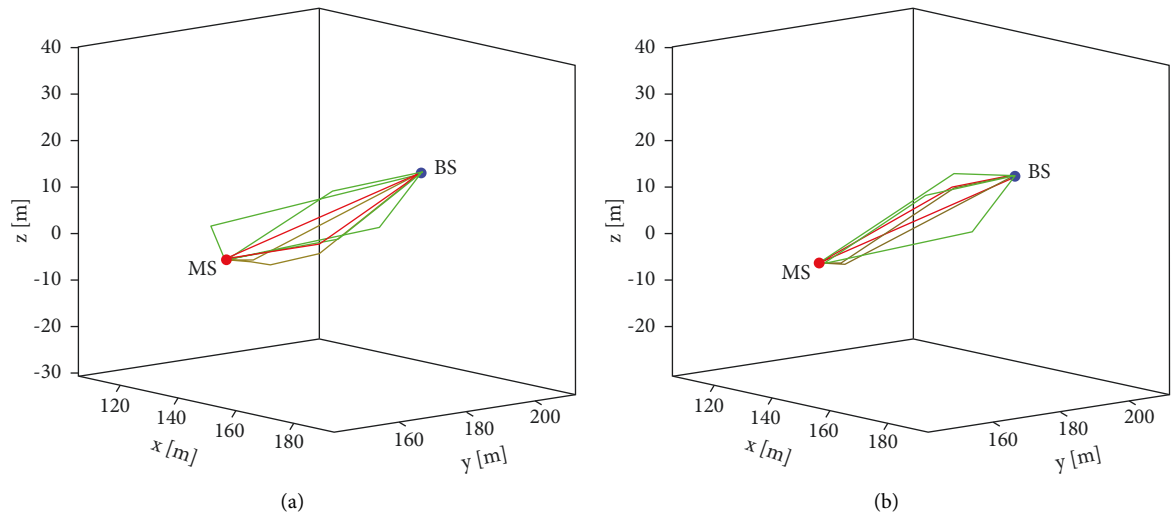

Figure 4: Diagrams of nonreciprocal beam patterns, the T-R separation distance is 72.8 m. (a) Downlink: BS beamwidth 30°, MS beamwidth 60°. (b) Uplink: BS beamwidth 60°, MS beamwidth 30°.

statistical histogram of the AoA results for all rays over this process. Besides, the widely used von Mises probability distribution function (PDF) is utilized to depict the AoA distribution and the fitting result is plotted in this figure. Clearly, this curve shows a good fitting trend to the simulated data. Considering that perfect beam alignment is achieved regardless of MS position and velocity, we focus on the angle between the LoS path and the arrival path from the last reflection bounce to the MS, abbreviated as quasi-AoA. For instance, as shown in Figure 3, α_1 and β_1 denote the AoD and AoA of the first ray path, whereas $\tilde{\alpha}_1$ and $\tilde{\beta}_1$ mean the corresponding quasi-AoD and quasi-AoA, respectively.

Based on this novel definition, the corresponding expression $\tilde{\alpha}_n$ of the n-th path is

$$\tilde{\alpha}_n = \arccos\left(\langle \vec{\Phi}_s^{\mathrm{D}} \cdot \vec{\Phi}_n^{\mathrm{D}} \rangle\right), \tag{14}$$

where $\vec{\Phi}_s^{\mathrm{D}}$ is the angle unit vector of Tx beam-steering direction with respect to α_s^H. Similarly, the expressions of $\vec{\Phi}^{\mathrm{A}}$, $\vec{\Phi}_s^{\mathrm{A}}$, and $\tilde{\beta}$ can also be derived.

Figure 5(b) plots the statistics results of the quasi-AoAs over the MS movement process. It can be observed that the majority appears at lower values and a tail comes into view at higher values. Remember that all values of quasi-AoAs are larger than 0. Taking these two factors into account, the gamma distribution is a promising candidate. Hence, we attempt to fit the results by using the gamma distribution function with a detailed expression as

$$f(\tilde{\beta}|a,b) = \frac{1}{b^a \Gamma(a)} \tilde{\beta}^{a-1} e^{-\tilde{\beta}/b}, \tag{15}$$

where a is the shape parameter, b is the scale parameter, and $\Gamma(\cdot)$ means the gamma function. As compared in Figure 5(b), the gamma distribution is a better option with a lower root mean squared error (RMSE) result. This angular distribution model provides insights into the angular generation for current prevailing channel models like GBSM.

The Doppler frequency shift is another pivotal parameter for a ray. It can be calculated as

$$\nu_n = \frac{v_{\mathrm{MS}}}{\lambda} \cos\left(\tilde{\beta} \pm \beta_0 - \gamma_{\mathrm{MS}}\right), \tag{16}$$

where β_0 means the AoA of the LoS link, symbol " $\pm$ " depends on the relative position of BS and MS, and γ_{MS} is the movement direction of MS.

4.2. Joint Distribution of Quasi-AoAs and Quasi-AoDs. In this subsection, we aim to characterize the distribution of quasi-AoDs. We try to obtain its distribution based on the prior distribution of quasi-AoAs. To characterize the joint distribution relationship between quasi-AoAs and quasi-AoDs, we make statistics of those rays up to 3 reflection bounces since that those high-bounce rays contribute little power to the received signal. The statistical histogram results of these rays are scattered in Figure 6(a), where the abscissa and ordinate mean quasi-AoA and quasi-AoD, respectively. For a certain bin, the lighter color it is, the higher probability it means. From this figure, we can draw two conclusions. First, the movement of vehicles leads to discernible trajectories with different lifetimes, which demonstrates the channel evolution. Usually, it can be characterized from a perspective of the birth-death process [36]. Second, the distribution result indicates that quasi-AoAs and quasi-AoDs are not irrelevant to each other. Two dense clusters with irregular shapes can be recognized roughly. Herein, we adopt the GMM to depict this joint probability distribution, which can be expressed as

$$P(\vec{x};\theta) = \sum_{k=1}^{K} \rho_k \phi(\vec{x}|\theta_k), \tag{17}$$

$$0 \le \tilde{\alpha} \le 0.5\alpha_W, \tag{18}$$

$$0 \le \tilde{\beta} \le 0.5\beta_W, \tag{19}$$

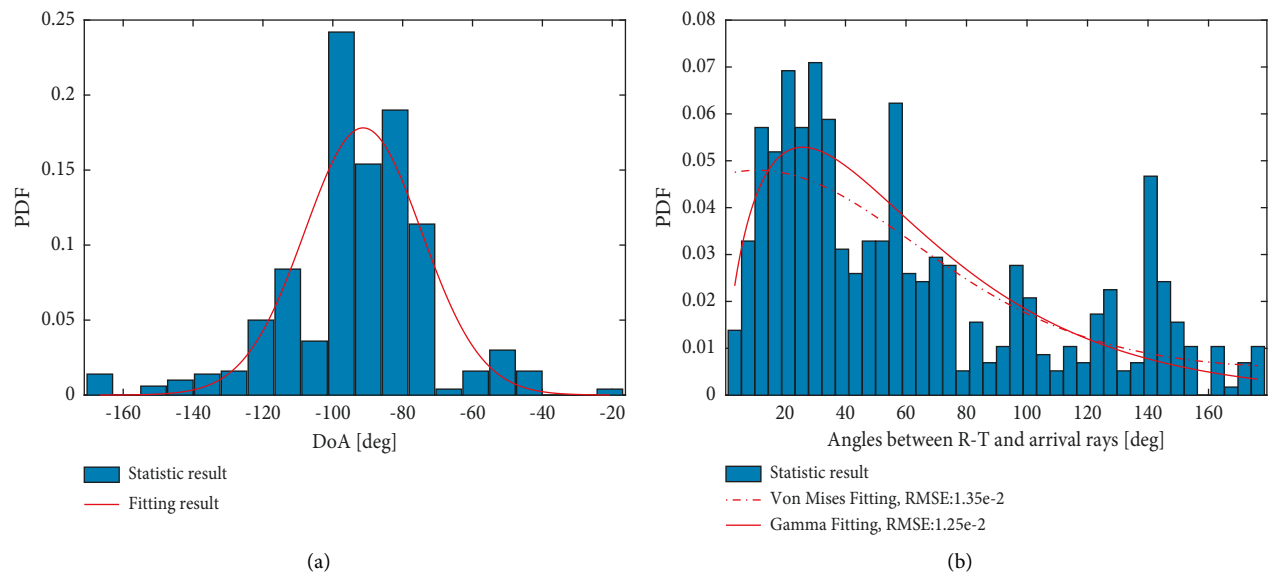

Figure 5: Comparisons of two angular statistics, (a) AoAs and (b) quasi-AoAs.

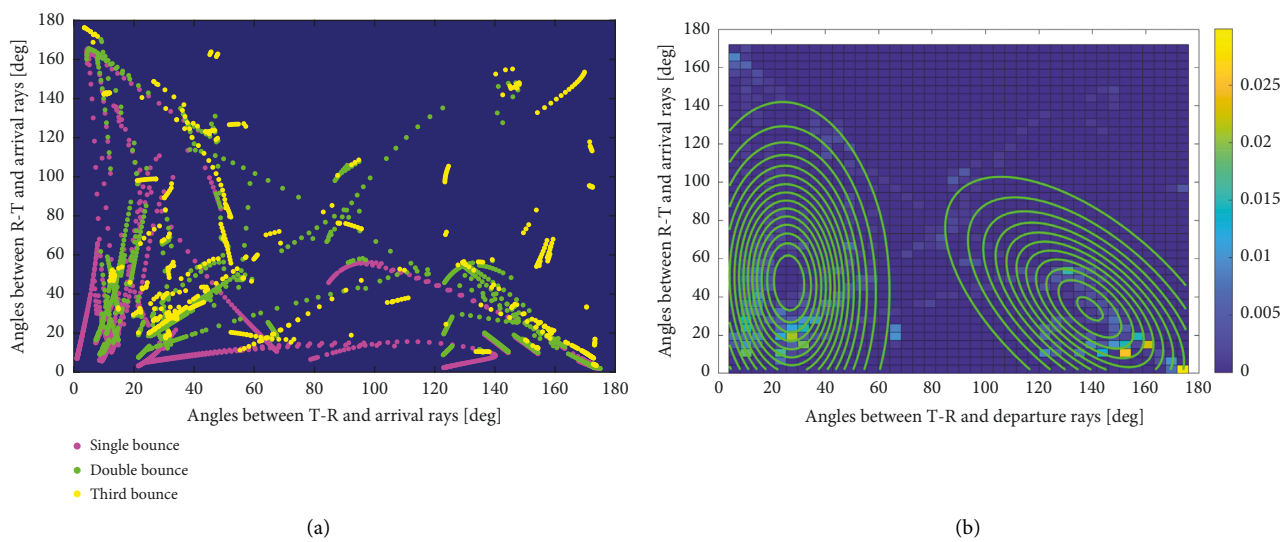

Figure 6: Statistics results of (a) angular trajectories of rays; (b) histogram of quasi-AoAs and quasi-AoDs.

where (18) and (19) denote the beamwidth constraints under the condition of perfect beam alignment. As illustrated in equation (11), beams act like spatial filters regarding rays with different AoAs and AoDs. Therefore, only a few rays survive when considering beamforming as presented in Figure 4. Under this case, the statistical results will be less accurate as a result of few samples. Consequently, the GMM-based joint distribution of multiple rays is obtained based on the omnidirectional antenna, and the nonreciprocal beams are considered as constraints since that perfect beam alignment is assumed in this paper.

A data point consists of two variables $\vec{x} = (\tilde{\alpha}, \tilde{\beta})$, K is the cluster number, which can be determined by the Akaike information criterion (AIC). The k-th component has a mixing proportion ρ_k, a mean of $\vec{\mu_k}$, and a covariance matrix of Σ_k for this multivariate case. Parameter θ_k can be expressed as $\theta_k = \{\vec{\mu_k}, \Sigma_k\}$ and $\phi(\vec{x}|\theta_k)$ refers to the k-th component, which can be calculated by

$$\phi(\vec{x}|\theta_k) = \frac{1}{\sqrt{2\pi|\Sigma_k|}} e^{-(\vec{x}-\vec{\mu}_k)^T \Sigma_k^{-1} (\vec{x}-\vec{\mu}_k)/2}, \tag{20}$$

where symbol $|\cdot|$ means the determinant operator, and Σ_k^{-1} indicates the inverse matrix of Σ_k. To obtain these 3 key parameters $(\rho_k, \vec{\mu}_k, \Sigma_k)$, the maximum likelihood estimation (MLE) is adopted to estimate from the mixture PDF. Assume that $\vec{X}_1, \ldots, \vec{X}_n$ are observed random variables obeying Gaussian distribution with unknow parameters, then the likelihood function is given as

$$L(\vec{X}; \theta) = \prod_{i=1}^{n} P\left(\vec{X}_i; \theta\right), \tag{21}$$

Table 4: GMM fitting results.

Parameters	Component index	Values
ρ	1	0.65
	2	0.35
μ	1	[22.545.8]
	2	[139.033.9]
Σ	1	$\begin{bmatrix} 309.6 & -10 \\ -10 & 1796 \end{bmatrix}$
	2	$\begin{bmatrix} 708.7 & -249.4 \\ -249.4 & 1243.6 \end{bmatrix}$

and the corresponding log likelihood function of equation (21) can be calculated as

$$\ln L(\vec{x};\theta_k) = \sum_{i=1}^{n} \ln\left(\sum_{k=1}^{K} \rho_k \phi(\vec{x}|\theta_k)\right). \tag{22}$$

By taking partial derivatives of equation (22) to maximize the likelihood, these 3 parameters can be obtained. When estimating, the expectation-maximum (EM) algorithm is usually adopted. Initially, the parameters are randomly chosen for the mixture model parameters $\theta_{1:K} = (\theta_1, \ldots, \theta_K)$. Then, the parameters are updated in each iteration, including E-stimation and M-aximization steps, until the convergence criteria are satisfied, whereas the E-step calculates the membership coefficients for all data point $(i = 1, \ldots, N)$ and mixture components $(k = 1, \ldots, K)$ by utilizing the current parameters $\theta_{1:K}$, i.e.,

$$\gamma_{ik} = \frac{\rho_k \phi\left(\vec{X}_i;\theta_k\right)}{\sum_{k=1}^{K} \pi_{ik} \phi\left(\vec{X}_i;\theta_k\right)}, \tag{23}$$

where γ_{ik} denotes the possibility of data $\vec{X}_i$ belonging to the k-th Gaussian model with an obvious constraint $\sum_{k=1}^{K} \gamma_{ik} = 1$. In terms of the M-step, it aims to calculate the coefficient and find the parameters, which can be expressed as

$$\begin{aligned} \rho_k^{\text{new}} &= \frac{\sum_{i=1}^{N} \gamma_{ik}}{N}, \\ \mathbb{E}[X_k]^{\text{new}} &= \frac{\sum_{i=1}^{N} \gamma_{ik} \vec{X}_i}{\sum_{i=1}^{N} \phi_{ik}} = \mu_k, \\ \text{Var}[X_k]^{\text{new}} &= \frac{\sum_{i=1}^{N} \gamma_{ik} \left(\vec{X}_i - \mathbb{E}[X_k]^{new}\right)^2}{\sum_{i=1}^{N} \phi_{ik}} = \Sigma_k^2, \end{aligned} \tag{24}$$

where $\mathbb{E}[\cdot]$ is the mathematical expectation operator, and $\text{Var}[\cdot]$ means the calculation of variance.

By adopting the GMM, Figure 6(b) presents the joint probability distribution histogram of quasi-AoAs and quasi-AoDs together with the GMM fitting results expressed in the contour style. The cluster number is set to 2 and the corresponding estimated parameters are listed in Table 4.

Once the quasi-AoA value $\tilde{\beta}$ of a ray is determined, the distribution of 2-dimensional GMM is reduced to 1-dimensional GMM. Consequently, the corresponding quasi-DoD value can be obtained by the Bayes estimation, i.e.,

$$\begin{aligned} f(\tilde{\alpha}|\tilde{\beta}) &= P\left(\tilde{\alpha}|\tilde{\beta}, \theta_{1:K}\right), \\ \tilde{\alpha}_0 &= \text{find}\left\{\text{seed} = \text{CDF}^{-1}(\tilde{\alpha}|\tilde{\beta})\right\}, \end{aligned} \tag{25}$$

where seed is a random number distributed evenly within the interval $(0, 1)$, and $\text{CDF}(\cdot)$ means the cumulative distribution function (CDF) of $f(\cdot)$. Once the $\tilde{\beta}$ is determined, the two-dimensional GMM is reduced to one-dimensional function. Hence, the $\text{CDF}(\cdot)$ is a sum of several error functions. Let $\phi(\tilde{\alpha}|\mu_{k|\tilde{\beta}}, \sigma_{k|\tilde{\beta}})$ denote the k-th Gaussian distribution component. Then, the corresponding total CDF can be expressed as

$$\text{CDF}(\tilde{\alpha}|\tilde{\beta}) = \sum_{k=1}^{K} \frac{\rho_k}{2}\left(1 + \text{erf}\left(\frac{\tilde{\alpha} - \mu_{k|\tilde{\beta}}}{\sigma_{k|\tilde{\beta}}}\sqrt{2}\right)\right), \tag{26}$$

where $\text{erf}(\cdot)$ means the error function. Obviously, it is hard to find the explicit expression of the inverse CDF; hence, numerical solution is used herein.

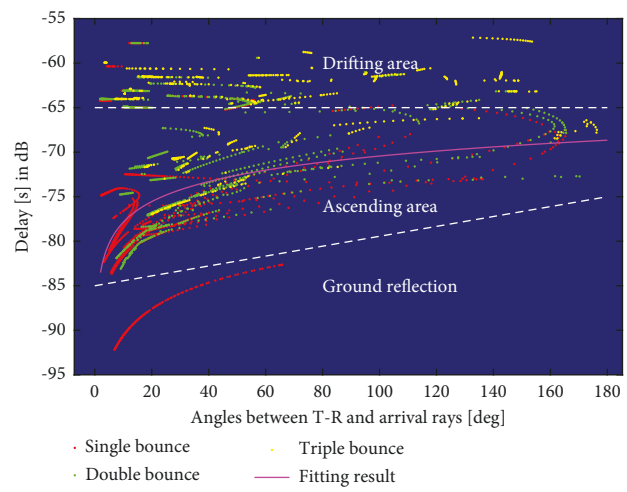

Figure 7: Relationship between quasi-AoAs and relative propagation delays.

4.3. Joint Distribution of Quasi-AoAs and Propagation Delay. Another crucial parameter for a path is the propagation delay/distance. In this section, we focus on characterizing the joint distribution between quasi-AoAs and the propagation distance. To better illustrate the scattered datapoints, we use the propagation delay in decibel instead of distance, and the corresponding results are presented in Figure 7. Generally speaking, these datapoints can be divided into 3 regions roughly by two dashed lines. The first part is the single-bounce trajectory at the bottom, which stems from the ground reflection. This part is a deterministic process that can be easily derived by some geometric manipulations. Those datapoints located in the middle region present an ascending trend, which is characterized by a power function with a time-varying variance. It is noteworthy that these datapoints mainly stem from single-bounce and double-

Table 5: A summary of the joint quasi-AoAs and delay models.

Properties	Ground area	Ascending area	Drifting area
Process	D	S	S
Expression	—	$y = \widehat{a}x^{\widehat{b}} + \mathcal{N}(0, \widehat{\sigma}^2)$	$\mathcal{N}(\widehat{\mu}, \widehat{\sigma}^2)$
Values	—	$\widehat{a} = -86.1, \widehat{b} = -4.4 \times 10^{-2}, \widehat{\sigma} = 3.3$	$\widehat{\mu} = -62.8, \widehat{\sigma} = 1.8$
Weight	—	0.61	0.39
X (dB)	3	6–9	9–18

D: deterministic; S: stochastic.

bounce reflections. In terms of the rest datapoints on the top, they exhibit a drifting status and we use the Gaussian distribution to depict them. Table 5 presents a summary of these 3 regions.

5. Conclusions

In this paper, we propose a 3-D geometric beam channel model based on the ray-tracing and conduct the angular distribution analysis based on the simulation results for multiple reflection bounces. Results reveal that the arrival angles between reflected rays and the LoS path, abbreviated as quasi-AoA, can be characterized by the gamma distribution with high accuracy. Then, the GMM is used to characterize the joint distribution between quasi-AoAs and quasi-AoDs. Furthermore, we analyze the relationship between quasi-AoAs and propagation delays. Consequently, nonreciprocal beam pattern channel modeling should take the joint angular distribution relationship into account seriously and our findings are important to beam channel models for next-generation mobile communications.

Data Availability

The simulation data used to support the findings of this study were supplied by Beijing Jiaotong University under license and so cannot be made freely available. Requests for access to these data should be made to Liu Liu, liuliu@bjtu.edu.cn.

Conflicts of Interest

The authors declare that they have no conflicts of interest.

Acknowledgments

This research was supported by the National Key Research and Development Program of China under grant 2020YFB1804901.

References

[1] R. He, B. Ai, G. Wang, M. Yang, C. Huang, and Z. Zhong, "wireless channel sparsity: measurement, analysis, and exploitation in estimation," *IEEE Wireless Communications*, vol. 28, no. 4, pp. 113–119, 2021.

[2] R. He, C. Schneider, B. Ai et al., "Propagation channels of 5G millimeter-wave vehicle-to-vehicle communications: recent advances and future challenges," *IEEE Vehicular Technology Magazine*, vol. 15, no. 1, pp. 16–26, 2020.

[3] T. S. Rappaport, Y. Xing, G. R. MacCartney, A. F. Molisch, E. Mellios, and J. Zhang, "Overview of millimeter wave communications for fifth-generation (5G) wireless networks-with a focus on propagation models," *IEEE Transactions on Antennas and Propagation*, vol. 65, no. 12, pp. 6213–6230, 2017.

[4] C. Guo, W. Hong, L. Tian et al., "Design and implementation of a full-digital beamforming array with nonreciprocal tx/rx beam patterns," *IEEE Antennas and Wireless Propagation Letters*, vol. 19, no. 11, pp. 1978–1982, 2020.

[5] W. Hong, J. Zhou, J. Chen, Z. Jiang, C. Yu, and C. Guo, "Asymmetric full-digital beamforming mmWave massive MIMO systems for B5G/6G wireless communications," in *Proceedings of the 2020 IEEE Asia-Pacific Microwave Conference (APMC)*, pp. 31-32, Hong Kong SAR, PR China, December 2020.

[6] C.-X. Wang, J. Huang, M. Hai, X. Gao, and X. You, "6G wireless channel measurements and models: trends and challenges," *IEEE Vehicular Technology Magazine*, vol. 15, no. 4, pp. 22–32, 2020.

[7] K. Guan, J. Moreno, B. Ai, C. B. Rodriguez, and B. Peng, "5g channel models for railway use cases at mmWave band and the path towards terahertz," *IEEE Intelligent Transportation Systems Magazine*, vol. 13, no. 3, pp. 146–155, 2021.

[8] D. Yan, K. Guan, D. He, B. Ai, and Z. Li, "channel characterization for vehicle-to-infrastructure communications in millimeter-wave band," *IEEE Access*, vol. 8, pp. 42325–42341, 2020.

[9] J. Weng, X. Tu, Z. Lai, S. Salous, and J. Zhang, "Indoor massive MIMO channel modelling using ray-launching simulation," *International Journal of Antennas and Propagation*, vol. 2014, Article ID 279380, 13 pages, 2014.

[10] M. K. Samimi and T. S. Rappaport, "3-D millimeter-wave statistical channel model for 5G wireless system design," *IEEE Transactions on Microwave Theory and Techniques*, vol. 64, no. 7, pp. 2207–2225, 2016.

[11] G. R. MacCartney and T. S. Rappaport, "Rural macrocell path loss models for millimeter wave wireless communications," *IEEE Journal on Selected Areas in Communications*, vol. 35, no. 7, pp. 1663–1677, 2017.

[12] X. Yin, C. Ling, and M.-D. Kim, "Experimental multipath-cluster characteristics of 28-GHz propagation channel," *IEEE Access*, vol. 3, pp. 3138–3150, 2015.

[13] J. Huang, C.-X. Wang, R. Feng, J. Sun, W. Zhang, and Y. Yang, "Multi-frequency mmWave massive MIMO channel measurements and characterization for 5G wireless communication systems," *IEEE Journal on Selected Areas in Communications*, vol. 35, no. 7, pp. 1591–1605, 2017.

[14] G. R. Maccartney, T. S. Rappaport, S. Sun, and S. Deng, "Indoor office wideband millimeter-wave propagation measurements and channel models at 28 and 73 GHz for ultra-dense 5G wireless networks," *IEEE Access*, vol. 3, pp. 2388–2424, 2015.

[15] A. I. Sulyman, A. Alwarafy, G. R. MacCartney, T. S. Rappaport, and A. Alsanie, "Directional radio propagation path loss models for millimeter-wave wireless networks in the 28-, 60-, and 73-GHz bands," *IEEE Transactions on Wireless Communications*, vol. 15, no. 10, pp. 6939–6947, 2016.

[16] A. Sayeed and J. Brady, "Beamspace MIMO channel modeling and measurement: methodology and results at 28GHz," in *Proceedings of the 2016 IEEE Globecom Workshops (GC Wkshps)*, pp. 1–6, Washington, DC, USA, December 2016.

[17] J. Huang, C.-X. Wang, H. Chang, J. Sun, and X. Gao, "Multi-frequency multi-scenario millimeter wave MIMO channel measurements and modeling for B5G wireless communication systems," *IEEE Journal on Selected Areas in Communications*, vol. 38, no. 9, pp. 2010–2025, 2020.

[18] D. Caudill, P. B. Papazian, C. Gentile, J. Chuang, and N. Golmie, "Omnidirectional channel sounder with phased-ArrayAntennas for 5G mobile communications," *IEEE Transactions on Microwave Theory and Techniques*, vol. 67, no. 7, pp. 2936–2945, 2019.

[19] V. Degli-Esposti, F. Fuschini, E. M. Vitucci, M. Barbiroli, and M. Zoli, "Ray-tracing-based mm-wave beamforming assessment," *IEEE Access*, vol. 2, pp. 1314–1325, 2014.

[20] Remcom, "Wireless InSite," 2021, https://www.remcom.com/wireless-insite-em-propagation-software.

[21] H. Jiang, M. Mukherjee, J. Zhou, and J. Lloret, "channel modeling and characteristics for 6G wireless communications," *IEEE Network*, vol. 35, no. 1, pp. 296–303, 2021.

[22] Fraunhofer Heinrich Hertz Institute, "Quadriga," 2021, https://quadriga-channel-model.de.

[23] C.-X. Wang, J. Bian, J. Sun, W. Zhang, and M. Zhang, "A survey of 5g channel measurements and models," *IEEE Communications Surveys & Tutorials*, vol. 20, no. 4, pp. 3142–3168, 2018.

[24] S. Wu, C.-X. Wang, e.-H. M. Aggoune, M. M. Alwakeel, and X. You, "A general 3-D non-stationary 5G wireless channel model," *IEEE Transactions on Communications*, vol. 66, no. 7, pp. 3065–3078, 2018.

[25] J. Bian, C.-X. Wang, X. Gao, X. You, and M. Zhang, "A general 3D non-stationary wireless channel model for 5G and beyond," *IEEE Transactions on Wireless Communications*, vol. 20, no. 5, pp. 3211–3224, 2021.

[26] H. Jiang, R. He, C. Ruan, J. Zhou, and D. Chang, "Three-dimensional geometry-based stochastic channel modeling for intelligent reflecting surface-assisted UAV MIMO communications," *IEEE Transactions on Vehicular Technology*, vol. 10, no. 12, pp. 2727–2731, 2021.

[27] H. Jiang, Z. Zhang, L. Wu, J. Dang, and G. Gui, "A 3-D non-stationary wideband geometry-based channel model for MIMO vehicle-to-vehicle communications in tunnel environments," *IEEE Transactions on Vehicular Technology*, vol. 68, no. 7, pp. 6257–6271, 2019.

[28] K. Mao, Q. Zhu, M. Song, B. Hua, W. Zhong, and X. Ye, "A geometry-based beamforming channel model for UAV mmWave communications," *Sensors*, vol. 20, no. 23, p. 6957, 2020.

[29] L. Tian, V. Degli-Esposti, E. M. Vitucci, and X. Yin, "Semi-deterministic radio channel modeling based on graph theory and ray-tracing," *IEEE Transactions on Antennas and Propagation*, vol. 64, no. 6, pp. 2475–2486, 2016.

[30] J. Chen, X. Yin, L. Tian, and M. Kim, "Millimeter-Wave channel modeling based on A unified propagation graph theory," *IEEE Communications Letters*, vol. 21, no. 2, pp. 246–249, 2017.

[31] S. Taravati and G. V. Eleftheriades, "Full-duplex nonreciprocal beam steering by time-modulated phase-gradient metasurfaces," *Physical Review Applied*, vol. 14, no. 1, Article ID 014027, 2020.

[32] R. Karimian, S. Taravati, M. D. Ardakani, S. Ahmadi, and M. E. Zaghloul, "Nonreciprocal-beam phased-array antennas based on transistor-loaded phase shifters," *IEEE Transactions on Antennas and Propagation*, vol. 69, no. 11, pp. 7572–7581, 2021.

[33] X. Yang, S. Jin, G. Y. Li, and X. Li, "Asymmetrical uplink and downlink transceivers in massive MIMO systems," *IEEE Transactions on Vehicular Technology*, vol. 70, no. 11, pp. 11632–11647, 2021.

[34] M. Yan, L. Tian, X. Wang, and C. Yang, "A high performance frequency synthesizer for nonreciprocal full-digital tx/rx beamforming array," in *Proceedings of the 2021 International Conference on Microwave and Millimeter Wave Technology (ICMMT)*, Nanjing China, May, 2021.

[35] C. L. Dolph, "A current distribution for broadside arrays which optimizes the relationship between beam width and side-lobe level," *Proceedings of the IRE*, vol. 34, no. 6, pp. 335–348, 1946.

[36] B. Zhang, Z. Zhang, R. He, G. Dahman, and J. Ding, "Measurement-based markov modeling for multi-link channels in railway communication systems," *IEEE Transactions on Intelligent Transportation Systems*, vol. 20, no. 3, pp. 985–999, 2019.